

Pharmacological activation of REV-ERBs is lethal in cancer and oncogene-induced senescence

Gabriele Sulli¹, Amy Rommel², Xiaojie Wang³, Matthew J. Kolar⁴, Francesca Puca⁵, Alan Saghatelian⁴, Maksim V. Plikus³, Inder M. Verma² & Satchidananda Panda¹

The circadian clock imposes daily rhythms in cell proliferation, metabolism, inflammation and DNA damage response^{1,2}. Perturbations of these processes are hallmarks of cancer³ and chronic circadian rhythm disruption predisposes individuals to tumour development^{1,4}. This raises the hypothesis that pharmacological modulation of the circadian machinery may be an effective therapeutic strategy for combating cancer. REV-ERBs, the nuclear hormone receptors REV-ERB α (also known as NR1D1) and REV-ERB β (also known as NR1D2), are essential components of the circadian clock^{5,6}. Here we show that two agonists of REV-ERBs—SR9009 and SR9011—are specifically lethal to cancer cells and oncogene-induced senescent cells, including melanocytic naevi, and have no effect on the viability of normal cells or tissues. The anticancer activity of SR9009 and SR9011 affects a number of oncogenic drivers (such as HRAS, BRAF, PIK3CA and others) and persists in the absence of p53 and under hypoxic conditions. The regulation of autophagy and *de novo* lipogenesis by SR9009 and SR9011 has a critical role in evoking an apoptotic response in malignant cells. Notably, the selective anticancer properties of these REV-ERB agonists impair glioblastoma growth *in vivo* and improve survival without causing overt toxicity in mice. These results indicate that pharmacological modulation of circadian regulators is an effective antitumour strategy, identifying a class of anticancer agents with a wide therapeutic window. We propose that REV-ERB agonists are inhibitors of autophagy and *de novo* lipogenesis, with selective activity towards malignant and benign neoplasms.

The cell-autonomous circadian clock pleiotropically coordinates a complex network of physiological processes¹. In both mice and humans, disruption of circadian rhythms increases cancer incidence^{1,7}. Given the unique ability of the circadian clock to directly control several pathways that are crucial for tumorigenesis^{2,8–11}, pharmacological modulation of circadian components may offer promising selective anticancer strategies.

REV-ERBs are haem-binding circadian clock components^{6,12,13} that act as repressors of processes involved in tumorigenesis, including metabolism^{5,14,15}, proliferation¹⁶ and inflammation². Binding to tetrapyrrole haem enhances the repressive function of REV-ERBs¹³. The development of the pyrrole derivatives SR9009 and SR9011¹⁴ as specific agonists of REV-ERBs, with potent *in vivo* activity, prompted us to investigate whether pharmacological activation of these circadian repressors affects cancer cell viability by restraining pathways that are aberrantly activated in cancer.

SR9009 had a cytotoxic effect on cancer cells derived from a range of tumour types, namely brain cancer, leukaemia, breast cancer, colon cancer and melanoma (Fig. 1a, d, g, j, o). SR9011 displayed similar cytotoxic properties against the same cancer cell lines (Extended Data Fig. 1a–j). Notably, SR9009 and SR9011 are effective against tumour cell lines that harbour a range of oncogenic drivers, including HRAS,

KRAS, BRAF, PTEN deficiency and β -catenin (Fig. 1, Extended Data Fig. 1), but have little or no toxic effect on normal cells at comparable concentrations (Fig. 1a, b, Extended Data Fig. 1a, b). Therefore, the antitumour activity of REV-ERB agonists is not limited to a single oncogenic driver, but is instead effective against a broad spectrum of tumorigenic pathways.

Levels of REV-ERB mRNA are comparable between normal cells and their transformed counterparts (Fig. 1c). The anticancer activity of SR9009 and SR9011 is abolished following the downregulation of REV-ERBs by multiple short hairpin RNAs (shRNAs) (Fig. 1o, p, Extended Data Fig. 1d, l).

The impairment of cancer cell viability on treatment with SR9009 and SR9011 is due to induction of apoptosis, as assessed by cleaved caspase 3 and terminal deoxynucleotidyl transferase (TdT) dUTP nick-end labelling (TUNEL) assays and further verified by electron microscopy (Fig. 1e, f, h, i, k, l, Extended Data Fig. 1g–k). As the tumour suppressor p53 has an important role in apoptosis and is often inactivated in cancer, we tested whether the induction of apoptosis by agonists of REV-ERBs requires p53. Agonist-induced apoptosis was largely intact in cells with compromised p53 function (mutation, deletion or shRNA-mediated downregulation; Fig. 1a, b, Extended Data Fig. 2a–j), which indicates that the downstream apoptosis trigger is independent of p53. Agonists of REV-ERBs do not, therefore, require the presence of wild-type p53 and are effective against several oncogenic pathways; these observations expand the potential therapeutic repertoire of agonists of REV-ERBs against multiple tumour types.

The selectivity of agonists of REV-ERBs towards cancer cells suggests that SR9009 and SR9011 may affect cellular processes that are critical specifically for the survival of tumour cells, and not essential for normal cells. The increased production of reactive oxygen species (ROS) is detrimental specifically to cancer cells¹⁷, insofar as normal cells exhibit a greater tolerance for increased ROS production than do cancer cells. Agonists of REV-ERBs and other circadian clock components regulate mitochondrial metabolism and its oxidative activity^{15,18}. If ROS overproduction is involved in the enhanced sensitivity of cancer cells to agonists of REV-ERBs, lowering oxidative stress would protect them against the agonists. We co-treated cancer cells with agonists of REV-ERBs and the antioxidant *N*-acetyl-L-cysteine (NAC). As a second way of lowering oxidative stress, we administered agonists of REV-ERBs under hypoxic conditions. In neither experimental setting was the ability of agonists of REV-ERBs to trigger apoptosis in cancer cells impaired (Extended Data Figs 2k–n, 3), which suggests that excessive ROS production is not involved in the enhanced sensitivity of cancer cells to these agonists.

Next we investigated whether agonists of REV-ERBs target anabolic pathways that are selectively critical for cancer cell survival. REV-ERBs tightly control lipid metabolism by repressing several lipogenic enzymes, including fatty acid synthase (FAS) and stearyl-CoA

¹Regulatory Biology Laboratory, Salk Institute for Biological Studies, La Jolla, California 92037, USA. ²Laboratory of Genetics, Salk Institute for Biological Studies, La Jolla, California 92037, USA. ³Department of Developmental and Cell Biology, University of California, Irvine, Irvine, California 92697, USA. ⁴Clayton Foundation Laboratories of Peptide Biology, Salk Institute for Biological Studies, La Jolla, California 92037, USA. ⁵Department of Genomic Medicine, The University of Texas MD, Anderson Cancer Center, Houston, Texas 77030, USA.

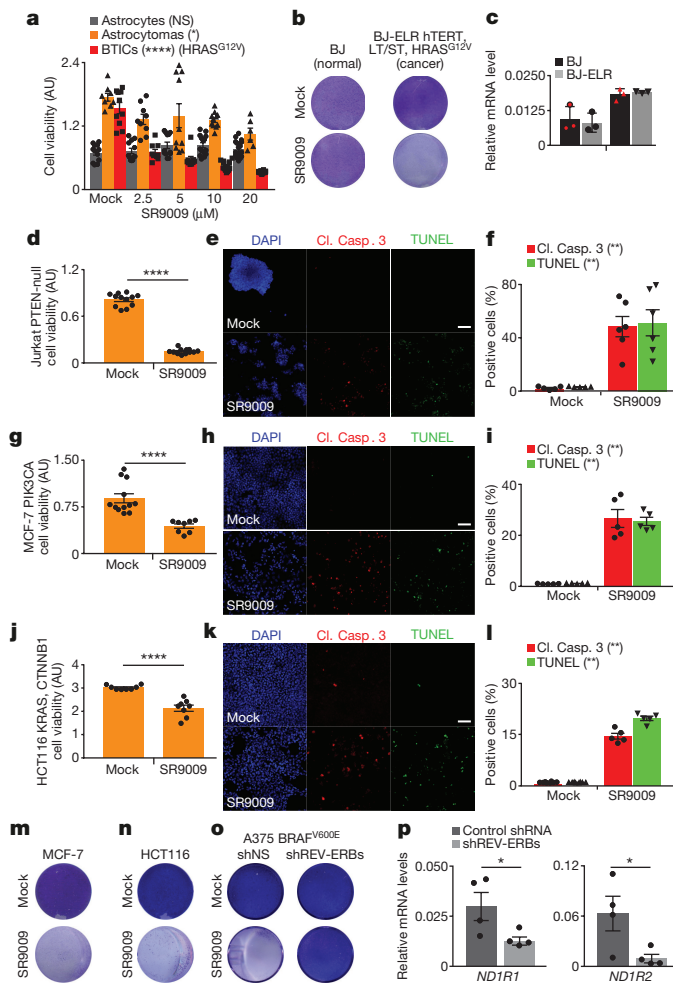


Figure 1 | SR9009 is selectively lethal in cancer cell lines driven by different oncogenic signalling. **a**, SR9009 treatment is cytotoxic specifically in cancer cells (72 h). One-way ANOVA. *n* indicates biological replicates: astrocytes, *n* = 12 (mock), *n* = 12 (2.5 μM), *n* = 12 (5 μM), *n* = 15 (10 μM), *n* = 18 (20 μM); astrocytomas, *n* = 8 (mock), *n* = 9 (2.5 μM), *n* = 10 (5 μM), *n* = 11 (10 μM) and *n* = 6 (20 μM), **P* = 0.037; and brain-tumour-initiating cells (BTICs), *n* = 10 (mock), *n* = 9 (2.5 μM), *n* = 9 (5 μM), *n* = 15 (10 μM) and *n* = 18 (20 μM), *****P* < 0.0001. **b**, SR9009 treatment impairs the viability of BJ-ELR, but not BJ, cells (proliferation assay, 7 days, 20 μM). LT/ST, large T antigen, small T antigen. **c**, Expression of REV-ERBs in BJ and BJ-ELR cells; quantitative PCR with reverse transcription (qRT-PCR), *n* = 3 biologically independent samples, two-tailed Mann–Whitney test. Expression of mRNA shown relative to housekeeper *RPLP0*. **d**, Jurkat cell viability is reduced by SR9009; *n* = 12 biological replicates, 72 h 20 μM, one-tailed Mann–Whitney test, *****P* < 0.0001. **e**, **f**, Immunostaining (**e**) and quantification (**f**) of cleaved caspase 3 (Cl. Casp. 3) and TUNEL assays (72 h, 20 μM); in **f**, *n* = 5 (mock) and 6 (SR9009) biologically independent samples, one-tailed Mann–Whitney test, cleaved caspase 3 assay, ***P* = 0.0022; TUNEL assay, ***P* = 0.0022. **g**, Breast cancer cell line MCF-7 viability is reduced by SR9009; *n* = 12 (mock) or 8 (SR9009) biological replicates, 72 h 20 μM, one-tailed Mann–Whitney test, *****P* < 0.0001. **h**, **i**, Immunostaining (**h**) and quantification (**i**) of cleaved caspase 3 and TUNEL assays (72 h, 20 μM). In **i**, *n* = 5 biologically independent samples, one-tailed Mann–Whitney test; cleaved caspase 3 assay, ***P* = 0.004; TUNEL assay, ***P* = 0.004. **j**, Colon cancer cell line HCT116 viability is reduced by SR9009; *n* = 8 biological replicates, water-soluble tetrazolium salt (WST-1) assay, 72 h, one-tailed Mann–Whitney test, *****P* < 0.0001. **k**, **l**, Induction of apoptosis is shown by cleaved caspase 3 and TUNEL staining (**k**, 72 h, 20 μM); for quantification in **l**, *n* = 8 (mock) or 5 (SR9009) biologically independent samples, one-tailed Mann–Whitney test; cleaved caspase 3 assay, ****P* = 0.0008; TUNEL assay ***P* = 0.0021. **m–o**, Prolonged SR9009 treatment eradicates cancer cells (7 days, 20 μM), but does not affect cells that express *NR1D1* and *NR1D2* shRNA. shNS, non-silencing shRNA. **p**, *NR1D1* and *NR1D2* qRT-PCR; *n* = 4 biologically independent samples; one-tailed Mann–Whitney test, **P* = 0.0286. NS, not significant. AU, arbitrary unit, shREV-ERBs, *NR1D1* and *NR1D2* shRNA. Scale bars, 50 μm. All panels representative of three biologically independent experiments. Data are mean ± s.e.m., except **c**, mean ± s.d.

desaturase 1 (SCD1)¹⁴. Unlike normal cells, cancer cells are highly dependent on *de novo* lipogenesis; major efforts are underway to develop cancer therapeutics on the basis of specific inhibitors of FAS and SCD1¹⁹. Agonists of REV-ERBs strongly reduced both mRNA and protein expression of these two key rate-limiting enzymes, which are involved in *de novo* lipogenesis (Extended Data Fig. 4a, b). This reduction led to the perturbation of several fatty acids and phospholipids (Extended Data Fig. 4c–i). Because oleic acid is the final product of SCD1 (Extended Data Fig. 4j), we investigated whether supplementing culture medium with oleic acid could attenuate the anticancer activity of agonists of REV-ERBs. Oleic acid impaired the anticancer activity of REV-ERB agonists (Extended Data Fig. 4k) but did not completely abrogate cytotoxicity, which suggests the involvement of additional mechanisms. By contrast, palmitic acid supplementation did not confer any protection (Extended Data Fig. 4l).

Cancer cells deal with their high metabolic demands through complex metabolic rewiring that involves the hyperactivation of autophagy²⁰. Autophagy is essential for cancer cell survival, whereas normal cells depend on this catabolic cellular process only in starvation conditions²⁰. Accordingly, inhibition of autophagy is a promising therapeutic strategy. However, chloroquine and its derivatives, which are the most common autophagy inhibitors, lack specificity and are toxic at high doses, potentially limiting their utility in clinical settings²¹.

Autophagy is modulated in a circadian fashion and is controlled by *NR1D1*^{15,22}. These observations prompted us to investigate whether the inhibition of autophagy is involved in the anticancer activity of agonists of REV-ERBs. We initially analysed the autophagosome marker LC3B to investigate whether agonists of REV-ERBs affect the numbers of autophagosomes; both SR9009 and SR9011 reduced the number of autophagosomes (Fig. 2a, b, Extended Data Fig. 5a, b). This decrease

in autophagosomes suggests that the administration of agonists of REV-ERBs inhibited autophagy. To expand upon this observation, we tested whether p62 (also known as sequestosome-1), which is a protein that is specifically degraded by autophagy, accumulates following treatment with agonists of REV-ERBs. These agonists induced a marked accumulation of p62 in a range of cancer cell lines. (Fig. 2c–e, Extended Data Fig. 5c–e). If autophagy has a dominant role in the induction of apoptosis triggered by agonists of REV-ERBs, autophagy inhibition should precede apoptosis induction: indeed, the blockage of autophagy shown by p62 accumulation occurred before the induction of apoptosis (Fig. 2f, g, Extended Data Fig. 5f, g). The inhibition of autophagy was further confirmed by analysis of the autophagic flux and by electron microscopy, with the latter showing that autophagosome formation was also impaired on starvation (Extended Data Fig. 6a–c). In addition, treatment with agonists of REV-ERBs prevented lysosome turnover, as shown by an increase in the lysosomal protein LAMP1 and by the enhanced activity of LysoTracker Red, which stains acidic vesicles (Extended Data Fig. 6d, e). The accumulation of lysosomes was also observed by transmission electron microscopy (Extended Data Fig. 6f). Together, these results indicate that agonists of REV-ERBs potentially inhibit autophagy.

When challenged with starvation, cancer cells are extremely sensitive to the inhibition of autophagy. The cytotoxicity of SR9009 and SR9011 was enhanced by starvation in a range of cancer cell lines (Fig. 2h, Extended Data Fig. 6g, h), which indicates the involvement of autophagy inhibition. Starvation did not induce the expression of REV-ERBs (Extended Data Fig. 6i, j), showing that autophagy inhibition is responsible for the increased sensitivity to agonists of REV-ERBs in starved cancer cells. Finally, the overexpression of core autophagy genes (*ULK2*, *ULK3* and *LKB1* (also known as *STK11*)) abrogated

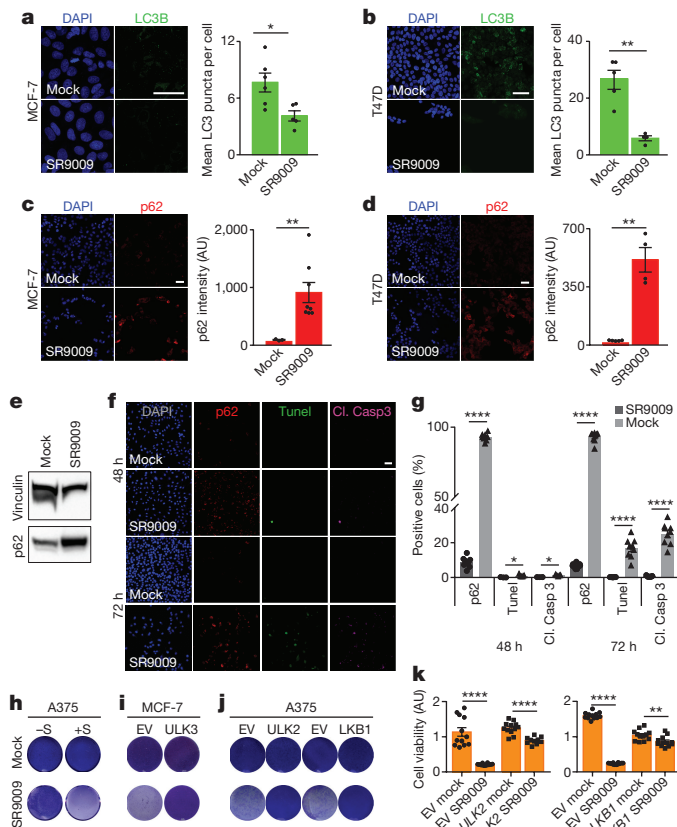


Figure 2 | SR9009 agonist of REV-ERBs inhibits autophagy.

a, b, SR9009 treatment reduces the number of autophagosomes, as shown by immunofluorescence of LC3B. *n* indicates biologically independent samples. MCF-7, *n* = 6 (mock) or 5 (SR9009); breast cancer cell line T47D, *n* = 5 (mock) or 4 (SR9009). One-tailed Mann–Whitney test; MCF-7 20 μ M 24 h, **P* = 0.0152, T47D 20 μ M 48 h, ***P* = 0.0079.

c, d, SR9009 induces accumulation of p62 as shown by immunofluorescence. *n* indicates biologically independent samples; MCF-7, *n* = 3 (mock) or 8 (SR9009); T47D, *n* = 5 (mock) or 4 (SR9009). One-tailed Mann–Whitney test; MCF-7 p62 48 h, ***P* = 0.0061; T47D 48 h, ***P* = 0.0079. **e**, Inhibition of autophagy is confirmed by the immunoblot for p62 (20 μ M, 48 h, melanoma cell line A375).

f, g, Inhibition of autophagy precedes apoptosis induction as shown by immunofluorescence of p62, cleaved caspase 3 and TUNEL assays. *n* indicates biologically independent samples. One-tailed Mann–Whitney test; A375 20 μ M, cleaved caspase 3 assay 48 h, *n* = 3, **P* = 0.0179; cleaved caspase 3 assay 72 h, *n* = 7, *****P* < 0.0001; TUNEL assay 48 h, *n* = 3, **P* = 0.0179; TUNEL assay 72 h, *n* = 7, *****P* < 0.0001; p62 48 h, *n* = 8, *****P* < 0.0001; p62 72 h, *n* = 9, *****P* < 0.0001. **h**, Starvation markedly accelerates the cytotoxic effect of the REV-ERB agonist SR9009 (A375, 3 days, 20 μ M, starvation time 24 h). **i**, Overexpression of *ULK3* impairs SR9009 induction of apoptosis (MCF-7, 6 days, 20 μ M). **j**, Overexpression of *ULK2* and *LKB1* impairs SR9009 induction of apoptosis (A375, 6 days, 20 μ M). **k**, WST-1 viability assay shows abrogation of apoptosis in *ULK2* (left panel) and *LKB1* (right panel) overexpressing cells (6 days). *n* indicates biological replicates. One-tailed Mann–Whitney test; left panel A375, 20 μ M, *n* = 12, empty vector (EV) mock versus EV SR9009, *****P* < 0.0001; *ULK2* mock (*n* = 12) versus *ULK2* SR9009 (*n* = 10), *****P* < 0.0001; right panel A375, *n* = 12, EV mock versus EV SR9009, *****P* < 0.0001; *LKB1* mock versus *LKB1* SR9009, ***P* = 0.0028. Scale bars, 50 μ m. All panels representative of three biologically independent experiments with similar results. All data are mean \pm s.e.m. For gel source data, see Supplementary Fig. 1.

induction of apoptosis in various tumour cell lines (Fig. 2i–k, Extended Data Fig. 6k–p).

Next, we sought to determine how agonists of REV-ERBs block autophagy. We initially compared differential autophagy outcomes observed between chloroquine and agonists of REV-ERBs. Chloroquine

inhibits autophagy at a late stage by blocking the fusion of autophagosomes and lysosomes, and thereby leads to the accumulation of autophagosomes (Extended Data Fig. 6a–c). By contrast, agonists of REV-ERBs decreased the number of autophagosomes, which suggests that they block autophagy at an early stage.

To gain additional mechanistic insights, we investigated whether agonists of REV-ERBs can regulate the expression of core autophagy genes. Analysis of a published report⁵ on chromatin occupancy of REV-ERBs revealed the presence of peaks in *Ulk3*, *Ulk1*, *Becn1* and *Atg7* (Extended Data Fig. 7a). Using HOMER software (<http://homer.ucsd.edu/homer/>), we found that NR1D1 and NR1D2 consensus binding sites were also present within these genetic loci (Extended Data Fig. 7b–e). Accordingly, *ULK3*, *ULK1*, *BECN1* and *ATG7* mRNAs and protein levels of ULK3, ULK1, BECN1 and ATG7 were downregulated on treatment with agonists of REV-ERBs, whereas the expression of these genes was induced following depletion of REV-ERBs by shRNA (Extended Data Figs 7f–j, 8a–e). Furthermore, in REV-ERB-depleted cells, agonists of REV-ERBs did not repress autophagy genes (Extended Data Figs 7k, 8f).

The activation of aberrant oncogenic stimuli is an early step in tumorigenesis. Oncogene-induced senescence (OIS) arises in normal cells to limit the expansion of cells affected by oncogenic stress^{23,24}. Although this provides an immediate benefit by arresting potentially dangerous cells, the accumulation of senescent cells over long periods of time contributes to tumour formation, tumour progression and age-related diseases²⁵. Furthermore, the induction of cellular senescence upon anticancer chemotherapy treatment promotes chemotherapy resistance and generates an environment that may support uncontrolled growth of neighbouring cells and fuel relapse²⁵; this highlights the need for senolytic agents. Although *de novo* lipogenesis is upregulated in cancer cells but not in OIS cells²⁶, an elevated level of autophagy is a known characteristic of OIS cells²⁷. Agonists of REV-ERBs are lethal when administered to cells characterized by oncogenic RAS signalling (Fig. 1, Extended Data Fig. 1), affect slowly proliferating cancer stem cells and potentially inhibit autophagy (Fig. 2, Extended Data Figs 5, 6, 8g–l).

We investigated whether treatment of OIS cells with agonists of REV-ERBs would block autophagy and lead to apoptosis. The overexpression of the HRAS proto-oncogene GTPase with the oncogenic mutation G12V (HRAS^{G12V}) (Extended Data Fig. 9a) established OIS, as shown by an increase in senescence-associated β -galactosidase activity and by upregulation of cell-cycle inhibitors (Extended Data Fig. 9b, c). Notably, agonists of REV-ERBs triggered the induction of apoptosis in OIS cells without affecting normal proliferating or quiescent cells (Fig. 3a–c, Extended Data Fig. 9d–g). In agreement with previous results (Fig. 2c–e, Extended Data Fig. 5c–e), treatment with agonists of REV-ERBs led to the accumulation of p62 and lysosomes and a reduction in autophagosomes (Fig. 3d, e, Extended Data Fig. 9h, i). Therefore, agonists of REV-ERBs inhibit autophagy in OIS cells. Finally, on overexpression of *ULK3*, the pro-apoptotic ability of the agonists of REV-ERBs was impaired (Fig. 3f). These results show that through their ability to block autophagy, these agonists can target a pre-malignant non-proliferating cellular population. Therefore, agonists of REV-ERBs display senolytic activity in addition to their oncolytic effects.

To understand whether agonists of REV-ERBs represent an effective therapeutic strategy, we investigated whether agonists of REV-ERBs affect OIS and tumour viability *in vivo*. Naevi are benign lesions consisting of cutaneous melanocytes that have undergone OIS upon aberrant activation of RAS signalling²⁸. Consistent with the *in vitro* observations discussed earlier, SR9009 treatment led to an increase in apoptosis in NRAS-induced naevi in mice, and the repression of autophagy genes (Fig. 4a–c, Extended Data Fig. 10a). This indicates the potential for non-proliferating premalignant cells to be selectively targeted by agonists of REV-ERBs *in vivo*. However, although naevi have been used as a model for studying OIS *in vivo*²⁸, they do not

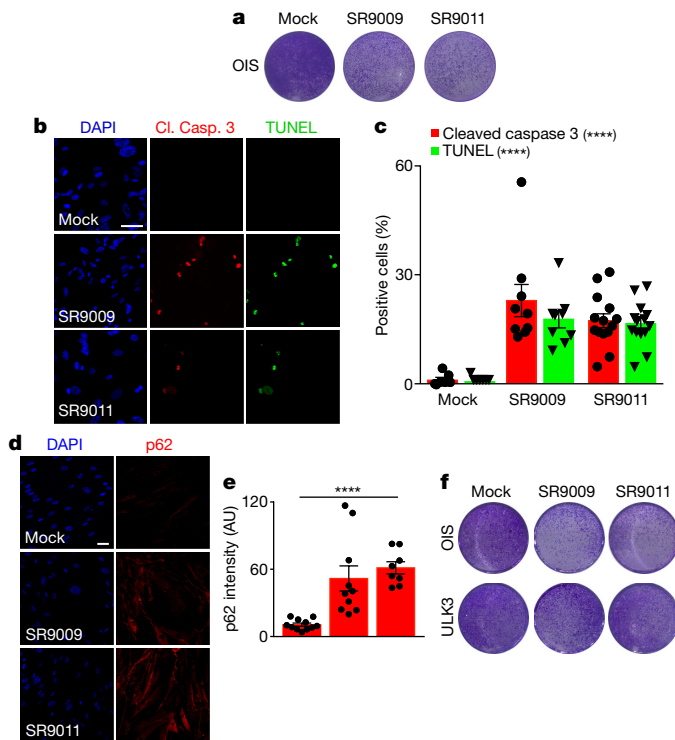


Figure 3 | SR9009 and SR9011 treatment evokes an apoptotic response and induces inhibition of autophagy in OIS cells. **a**, Proliferation assay shows that agonists of REV-ERBs impair viability of OIS cells (6 days, 20 μ M). **b**, **c**, Immunofluorescence assay for cleaved caspase 3 and TUNEL assay show apoptosis specifically in OIS cells. *n* indicates biologically independent samples; *n* = 7 (mock), *n* = 9 (SR9009) and *n* = 14 (SR9011). One-way ANOVA, 72 h, 20 μ M; cleaved caspase 3 assay, *****P* < 0.0001; TUNEL assay, *****P* < 0.0001; mean \pm s.e.m. **d**, **e**, p62 accumulates on treatment with agonists of REV-ERBs, as assayed by immunofluorescence for p62. *n* indicates biologically independent samples, *n* = 11 (mock), *n* = 10 (SR9009) and *n* = 8 (SR9011). One-way ANOVA, 72 h, 20 μ M, *****P* < 0.0001; mean \pm s.e.m. **f**, ULK3 overexpression protects OIS cells from cytotoxicity induced by agonists of REV-ERBs; 6 days, 20 μ M. Scale bars, 50 μ m. All panels representative of three biologically independent experiments with similar results.

affect neighbouring tissues and do not develop into melanomas: further studies are necessary to assess the therapeutic relevance of agonists of REV-ERBs as senolytic tools^{25,29}. As previously reported^{14,15}, agonists of REV-ERBs do not show overt toxicity; our TUNEL analyses—performed in normal skin and brain tissues—and our body weight analyses confirm this finding (Extended Data Fig. 10b–d). By contrast, established anticancer agents such as temozolomide are characterized by several side effects (Extended Data Fig. 10d).

SR9009 is known to cross the blood–brain barrier¹⁴, and several glioblastoma cell lines—including brain-tumour initiating cells (005 and RIGH), A172 and glioblastoma stem cells derived from patients—are sensitive to treatment with agonists of REV-ERBs *in vitro* (Fig. 1a, Extended Data Figs 1a, 2f, g, 8g and 10e). On analysis of REV-ERB status in glioblastoma data from The Cancer Genome Atlas (<http://www.cbioportal.org/>)^{30,31}, we observed that NR1D1 and NR1D2 status was unaltered in nearly all patients with glioblastoma (Extended Data Fig. 10f, and data not shown), which suggests a possible therapeutic use for agonists of REV-ERBs in clinical settings.

Finally, NR1D2 expression was positively correlated with survival in brain cancer patients (Fig. 4d, NR1D1 data are not available). For the above reasons, and because of the low toxicity of agonists of REV-ERBs, we tested SR9009 for treating brain tumours. Brain-tumour-initiating cells were transplanted into mouse brains by stereotaxic injection, and on tumour establishment, SR9009 treatment was initiated. SR9009 reduced glioblastoma growth, triggered apoptosis and downregulated

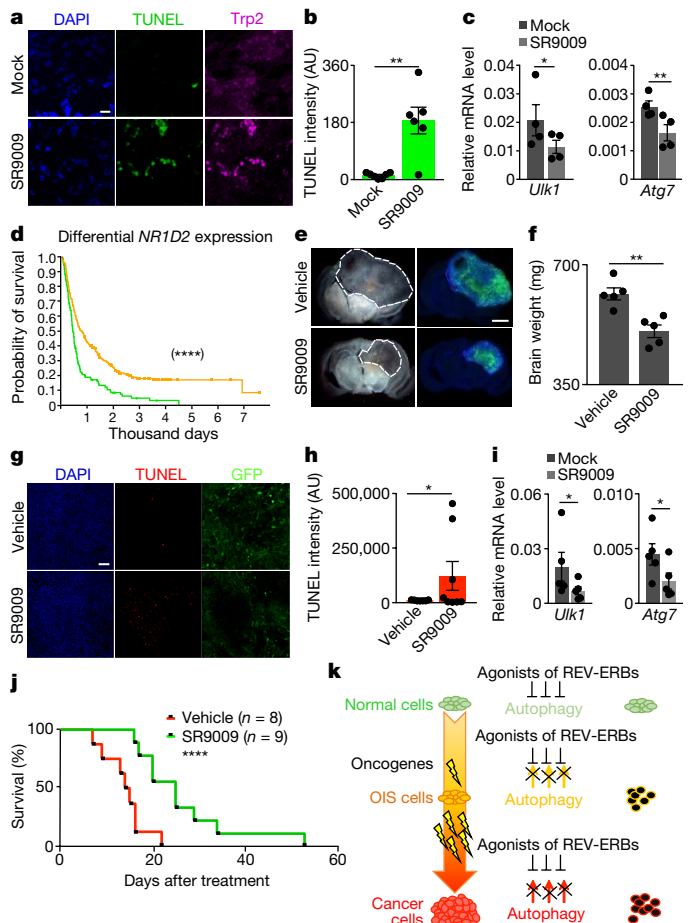


Figure 4 | SR9009 impairs viability of NRAS-driven naevi and glioblastoma growth and extends survival. **a**, **b**, SR9009 treatment induces apoptosis *in vivo* in NRAS-driven naevi, as assayed by immunofluorescence analysis (representative images of two independent experiments with similar results, TRP2 melanocytic marker and TUNEL assay; one-tailed Mann–Whitney test, ***P* = 0.0058. *n* indicates biologically independent samples, *n* = 7 (mock) and 6 (SR9009), 12 days of SR9009, 20 μ M, four mice. Scale bar, 10 μ m. **c**, Autophagy genes are downregulated after treatment of NRAS-driven naevi, *n* = 4 mice. One-tailed Mann–Whitney; *Ulk1*, **P* = 0.0249 and *Atg7*, ***P* = 0.007. **d**, NR1D2 expression correlates with survival in patients with brain cancer. *n* indicates biologically independent samples. Yellow line, intermediate expression (*n* = 224); green line, downregulated (*n* = 119). NIH Rembrandt database (<https://wiki.nci.nih.gov/display/ICR/Rembrandt+Data+Portal>); two-sided log-rank, *****P* < 0.0001. **e**, **f**, SR9009 treatment impairs *in vivo* growth of glioblastoma. Representative images of one experiment, *n* = 5 mice, 6 days, 200 mg kg⁻¹ SR9009 twice a day. One-tailed Mann–Whitney test, ***P* = 0.004. **g**, **h**, SR9009 induces apoptosis in glioblastoma, as shown by TUNEL assay; tumour cells are GFP-positive. Representative images of one independent experiment, 6 days 200 mg kg⁻¹ twice a day. One-tailed Mann–Whitney test, **P* = 0.02. *n* indicates biologically independent samples, *n* = 7 (mock) or 8 (SR9009), five mice. **i**, *In vivo* treatment with SR9009 results in downregulation of main autophagy genes. Six days, 200 mg kg⁻¹ twice a day, *n* = 5 mice. One-tailed Mann–Whitney test, **P* = 0.0476. **j**, SR9009 improves survival of mice affected by glioblastoma. SR9009, 100 mg kg⁻¹. Vehicle, *n* = 8; SR9009, *n* = 9 mice; two-tailed log-rank, *****P* = 0.0009. **k**, Scheme illustrating how agonists of REV-ERBs selectively affect OIS and cancer cells. All bar charts mean \pm s.e.m.

the expression of autophagy genes (Fig. 4e–i, Extended Data Fig. 10g). Additionally, SR9009 reduced tumour growth in a xenograft model of a patient-derived glioblastoma (Extended Data Fig. 10h, i). Most notably, SR9009 effectively and significantly improved survival in two glioblastoma models, including a xenograft derived from a patient (Fig. 4j, Extended Data Fig. 10j). The anticancer activity of SR9009 was

similar to that of temozolomide, the current therapeutic standard for glioblastoma (Extended Data Fig. 10j). Unlike temozolomide, however, SR9009 lacked toxicity.

Together, these results indicate that agonists of REV-ERBs are pharmacological tools that target a potentially wide spectrum of tumours and therapeutic windows, are highly selective and exhibit low toxicity (Fig. 4k). Importantly, REV-ERB agonists selectively target slowly proliferating tumorigenic and premalignant populations, such as naevi (Fig. 4k). We propose that the anticancer activity of agonists of REV-ERBs involves the inactivation of at least two cancer hallmarks³: *de novo* lipogenesis and autophagy, with autophagy—given its importance in meeting the metabolic demands of cancer cells—possibly having a major role. By simultaneously targeting two essential cancer hallmarks, agonists of REV-ERBs may represent an improved therapeutic strategy for treating cancer. These results strongly indicate that pharmacological modulation of circadian machinery is an innovative and selective strategy for cancer treatment (Fig. 4k).

Online Content Methods, along with any additional Extended Data display items and Source Data, are available in the online version of the paper; references unique to these sections appear only in the online paper.

Received 12 September 2016; accepted 24 November 2017.

Published online 10 January 2018.

- Fu, L. & Lee, C. C. The circadian clock: pacemaker and tumour suppressor. *Nat. Rev. Cancer* **3**, 350–361 (2003).
- Scheiermann, C., Kunisaki, Y. & Frenette, P. S. Circadian control of the immune system. *Nat. Rev. Immunol.* **13**, 190–198 (2013).
- Hanahan, D. & Weinberg, R. A. Hallmarks of cancer: the next generation. *Cell* **144**, 646–674 (2011).
- Straif, K. *et al.* Carcinogenicity of shift-work, painting, and fire-fighting. *Lancet Oncol.* **8**, 1065–1066 (2007).
- Cho, H. *et al.* Regulation of circadian behaviour and metabolism by REV-ERB- α and REV-ERB- β . *Nature* **485**, 123–127 (2012).
- Bugge, A. *et al.* REV-ERB α and REV-ERB β coordinately protect the circadian clock and normal metabolic function. *Genes Dev.* **26**, 657–667 (2012).
- Yu, E. A. & Weaver, D. R. Disrupting the circadian clock: gene-specific effects on aging, cancer, and other phenotypes. *Aging* **3**, 479–493 (2011).
- Plikus, M. V. *et al.* Local circadian clock gates cell cycle progression of transient amplifying cells during regenerative hair cycling. *Proc. Natl Acad. Sci. USA* **110**, E2106–E2115 (2013).
- Fu, L., Pelicano, H., Liu, J., Huang, P. & Lee, C. The circadian gene *Period2* plays an important role in tumor suppression and DNA damage response *in vivo*. *Cell* **111**, 41–50 (2002).
- Sancar, A. *et al.* Circadian clock control of the cellular response to DNA damage. *FEBS Lett.* **584**, 2618–2625 (2010).
- Bass, J. Circadian topology of metabolism. *Nature* **491**, 348–356 (2012).
- Preitner, N. *et al.* The orphan nuclear receptor REV-ERB α controls circadian transcription within the positive limb of the mammalian circadian oscillator. *Cell* **110**, 251–260 (2002).
- Yin, L. *et al.* REV-ERB α , a heme sensor that coordinates metabolic and circadian pathways. *Science* **318**, 1786–1789 (2007).
- Solt, L. A. *et al.* Regulation of circadian behaviour and metabolism by synthetic REV-ERB agonists. *Nature* **485**, 62–68 (2012).
- Woldt, E. *et al.* REV-ERB- α modulates skeletal muscle oxidative capacity by regulating mitochondrial biogenesis and autophagy. *Nat. Med.* **19**, 1039–1046 (2013).
- Vieira, E. *et al.* The clock gene *Rev-erb α* regulates pancreatic β -cell function: modulation by leptin and high-fat diet. *Endocrinology* **153**, 592–601 (2012).
- Gorrini, C., Harris, I. S. & Mak, T. W. Modulation of oxidative stress as an anticancer strategy. *Nat. Rev. Drug Discov.* **12**, 931–947 (2013).
- Peek, C. B. *et al.* Circadian clock NAD⁺ cycle drives mitochondrial oxidative metabolism in mice. *Science* **342**, 1243417 (2013).
- Currie, E., Schulze, A., Zechner, R., Walther, T. C. & Farese, R. V. Jr. Cellular fatty acid metabolism and cancer. *Cell Metab.* **18**, 153–161 (2013).

- White, E. Deconvoluting the context-dependent role for autophagy in cancer. *Nat. Rev. Cancer* **12**, 401–410 (2012).
- Rubinsztein, D. C., Codogno, P. & Levine, B. Autophagy modulation as a potential therapeutic target for diverse diseases. *Nat. Rev. Drug Discov.* **11**, 709–730 (2012).
- Ma, D., Panda, S. & Lin, J. D. Temporal orchestration of circadian autophagy rhythm by C/EBP β . *EMBO J.* **30**, 4642–4651 (2011).
- Serrano, M., Lin, A. W., McCurrach, M. E., Beach, D. & Lowe, S. W. Oncogenic *ras* provokes premature cell senescence associated with accumulation of p53 and p16^{INK4a}. *Cell* **88**, 593–602 (1997).
- Campisi, J. & d'Adda di Fagagna, F. Cellular senescence: when bad things happen to good cells. *Nat. Rev. Mol. Cell Biol.* **8**, 729–740 (2007).
- Childs, B. G. *et al.* Senescent cells: an emerging target for diseases of ageing. *Nat. Rev. Drug Discov.* **16**, 718–735 (2017).
- Quijano, C. *et al.* Oncogene-induced senescence results in marked metabolic and bioenergetic alterations. *Cell Cycle* **11**, 1383–1392 (2012).
- Young, A. R. *et al.* Autophagy mediates the mitotic senescence transition. *Genes Dev.* **23**, 798–803 (2009).
- Michaloglou, C. *et al.* BRAF^{E600}-associated senescence-like cell cycle arrest of human naevi. *Nature* **436**, 720–724 (2005).
- Chang, J. *et al.* Clearance of senescent cells by ABT263 rejuvenates aged hematopoietic stem cells in mice. *Nat. Med.* **22**, 78–83 (2016).
- Brennan, C. W. *et al.* The somatic genomic landscape of glioblastoma. *Cell* **155**, 462–477 (2013).
- Cancer Genome Atlas Research Network. Comprehensive genomic characterization defines human glioblastoma genes and core pathways. *Nature* **455**, 1061–1068 (2008).

Supplementary Information is available in the online version of the paper.

Acknowledgements We thank K. V. Ly, L. Fijany, Y. Soda, M. Soda and M. Schmitt for technical assistance; F. d'Adda di Fagagna, S. Minucci, A. Viale, G. Gargiulo and J. Karlseder for discussion and feedback; the Narita, Gage, Burris, Amati and Shaw laboratories, and F. F. Lang for reagents; and the Salk Institute's Waitt Advanced Biophotonics Center and Gene Targeting and Transfer, and M. Shokhirev and the Razavi Newman Integrative Genomics and Bioinformatics Core. G.S. is supported by the AIRC/Marie Curie International Fellowships in Cancer Research (12298), Istituto Superiore di Sanità, TRAIN 'Training through Research Application Italian iNitiative'. M.V.P. is supported by the NIH (NIAMS grants R01-AR067273 and R01-AR069653) and a Pew Charitable Trust grant. X.W. is supported by a CIHR postdoctoral fellowship (MFE-123724). I.M.V. is an American Cancer Society Professor of Molecular Biology. A.R. is supported by the NCI T32 grant, Salk Women in Science, Salk Excellerators Award and the Stavros Niarchos Foundation New Frontiers Salk Research Specialist Award. M.J.K. is supported by F30 DK112604. A.S. is supported by the NCI Cancer Center Support Grant P30 (CA014195 MASS core) and Dr. Frederick Paulsen Chair/Ferring Pharmaceuticals. This work was supported in part by a Worldwide Cancer Research grant and an American Federation of Aging Research mid-career grant M14322 to S.P. Additional support came from a Cancer Center Core Grant (P30 CA014195-38), the H. N. and Frances C. Berger Foundation, the Glenn Center for Aging Research and the Leona M. and Harry B. Helmsley Charitable Trust (grant #2012-PG-MED002).

Author Contributions X.W. and M.V.P. performed experiments related to naevi. A.R. participated in xenograft experiments. F.P. performed experiments in Extended Data Figs 8g–i, 10h–j. M.J.K. performed lipidomic assays. G.S. designed the study, performed experiments, analysed data and wrote the manuscript. A.S., I.M.V. and M.V.P. supervised experiments and edited the manuscript. S.P. supervised, designed the study and reviewed the data and manuscript. All authors discussed the results and commented on the manuscript.

Author Information Reprints and permissions information is available at www.nature.com/reprints. The authors declare no competing financial interests. Readers are welcome to comment on the online version of the paper. Publisher's note: Springer Nature remains neutral with regard to jurisdictional claims in published maps and institutional affiliations. Correspondence and requests for materials should be addressed to G.S. (gsulli@salk.edu) and S.P. (satchin@salk.edu).

Reviewer Information Nature thanks S. Kay, L. Zender and the other anonymous reviewer(s) for their contribution to the peer review of this work.

METHODS

Cell culture and treatments. BJ, WI38, BJ-ELR, A375, Jurkat, MCF7, T47D, HCT116, Becker (astrocytoma line, JCRB Cell Bank), PANC-1 and SK-MEL28 cells were grown under standard tissue-culture conditions and obtained through ATCC. No further authentication was performed. HCT116 p53^{-/-} cells were a gift from B. Amati. BTICs (005, RIGH) were cultured as previously described³². OIS cells were generated as previously described³³. Quiescent cells were obtained by contact inhibition. Cell lines were tested for mycoplasma contamination. Senescence-associated (SA)- β -galactosidase assay (Cell Biolabs) was performed as previously described³³. SR9009 (Xcessbio, Millipore) and SR9011 (Xcessbio) were dissolved in DMSO for *in vitro* studies and for ear topical administration; SR9009 and temozolomide (Cayman Chemicals) were dissolved in 15% Cremophor (Sigma-Aldrich) in sterile water for *in vivo* studies. Hypoxia was induced by lowering incubator oxygen percentage to 1–2%, or with NAC supplementation in the medium (10 mM; Sigma-Aldrich); EBSS (Life Technologies) was used to induce starvation. Proliferation assays were performed to assess the cytotoxicity of SR9009 and SR9011 in normal and cancer cells by using crystal violet and cell proliferation reagent WST-1 (Roche); all treatment started when cells were 80% confluent (except for the BTIC experiments). MTS (3-(4,5-dimethylthiazol-2-yl)-5-(3-carboxymethoxyphenyl)-2-(4-sulfophenyl)-2H-tetrazolium) assays were performed according to the manufacturer's instructions (CellTiter 96 Aqueous One, Promega).

Human samples. Glioblastoma stem cells (GSCs) were isolated from specimens from patients with glioblastoma, who had undergone surgery at the University of Texas MD Anderson Cancer Center (UTMDACC)³⁴. The diagnosis of glioblastoma was established by histological examination, according to the WHO (World Health Organization) classification. Samples derived from patients were obtained with the consent of patients, under an ethically approved Institutional Review Board protocol LAB04-0001 chaired by F. F. Lang (UTMDACC). Tumour specimens were dissociated and resuspended in Dulbecco's modified Eagle's medium/F12 (Gibco) supplemented with B27 ($\times 1$, Invitrogen), bFGF (20 ng ml⁻¹ Peprotech), and EGF (20 ng ml⁻¹, Peprotech). Cells were cultured as neurospheres and passaged every 5–7 days, on the basis of sphere size.

Plasmids. pBABE-Puro and pBABE-Puro H-RasV12 were used as previously described³³. pLKO.1 *NR1D1* shRNA (shNR1D1), pLKO.1 *NR1D2* shRNA (shNR1D2) (Sigma-Aldrich), pLPCULK3, pLPCLC3B (gift from the Narita laboratory) pLenti-ULK2 (ABM), pBABE-LKB1 (gift from the Shaw laboratory) were obtained as indicated. shNR1D1 no. 1: CCGGGCGCTTTGCTTCGTTGTTCAACTCGAGTTGAACAACGAAGCAAAGCGCTTTTT; shNR1D1 no. 2: CCGCCAGCCCTGAATCCCTCTATACTCGAGTATAGAGGGATTACAGGGCTGTTTTT; shNR1D2 no. 1: CCGGGCCCTCCAACCTTAGTGTGAAGCTGAGTTCATCACTAAGTTGGAGGGCTTTTT; shNR1D2 no. 2: CCGGCCAGTACAAGAAGTGCCTGAACCTCGAGTTCAGGCACCTTCTGTACTGTTTTT.

Immunofluorescence microscopy. For brain-tissue immunofluorescence, all mice were perfused with 0.9% NaCl followed by 4% paraformaldehyde in PBS. The brains were collected, fixed overnight and transferred to 30% sucrose in PBS. For fluorescent staining, 40- μ m coronal sections on a sliding microtome were prepared and imaged with the Zeiss LSM 780 Side Port Laser Scanning Confocal microscope. Mouse ears were fixed in 4% paraformaldehyde and subjected to histology. Paraffin-embedded sections were stained with anti-TRP2 at 2 μ g ml⁻¹ (Santa Cruz), TUNEL *In Situ* Cell Death Detection Kit, Fluorescein (Roche). Cells were fixed and probed as previously described³³. Images and confocal sections were acquired using the Zeiss LSM 780 Side Port Laser Scanning Confocal microscope. Comparative immunofluorescence microscopy analyses were performed in parallel, with identical acquisition and analysis parameters. ImageJ software (v1.49g) was used to perform quantitative analyses and to assay intensity differences. To count LC3B puncta, after selecting a threshold to minimize any effect of background signal analyses were performed on projected stack using the ImageJ function 'analyse particles'. 3D Objects Counter was used to analyse intensity. Apoptosis was evaluated by the immunostaining of cleaved caspase 3 (Cell Signaling No. 9664 1:200), and by TUNEL assay using *In Situ* Cell Death Detection Kit, Fluorescein or TMR red (Roche). Antibodies used were LC3B (Cell Signaling No. 3868 1:200), Lamp1 (Cell Signaling #9091 1:200), Sqstm1/p62 (Abcam ab56416 1:100), Sqstm1/p62 (MBL PM045) and Ras (BD #610002, 1:200). LysoTracker Red DND-99 (Lifetech) was used to visualize lysosomes.

Electron microscopy. Cells grown on ACLAR coverslips were fixed in 2.5% glutaraldehyde with 2% paraformaldehyde in 0.15 M cacodylate buffer containing 2 mM calcium chloride, pH 7.4, at 37°C for five minutes, followed by an hour at 4°C. The coverslips were then washed in 0.15 M cacodylate buffer containing 2 mM calcium chloride, and secondarily fixed in 1% osmium tetroxide and 0.3% potassium ferrocyanide in the same buffer. Subsequently, the coverslips were washed in water and stained en bloc with 2% uranyl acetate, followed by a graded dehydration in ethanol (35%, 50%, 70%, 90%, 100% and 100%). Samples were then rapidly

infiltrated in EPON resin using a Pelco BioWave microwave processing unit (Ted Pella), flat embedded and cured at 60°C overnight. Regions of interest were excised and remounted on blank resin stubs. Ultrathin (70 nm) sections were then cut on a UC7 ultramicrotome (Leica) and cells were imaged on a transmission electron microscope at 120 kV (Zeiss Libra 120 PLUS).

Immunoblotting. Cells were lysed in sample buffer and 20–50 μ g of whole cell lysate was resolved by gel electrophoresis (Bolt 4–12% Bis-Tris Plus Gels, Life Technologies), transferred to nitrocellulose (iBlot Transfer Stack, nitrocellulose, Life Technologies) and probed with the following antibodies: anti-cleaved caspase 3 (1:250 Cell Signaling No. 9664); anti-vinculin clone hVIN-1 (SIGMA; 1:10,000), anti Sqstm1/p62 (Abcam ab56416; 1:500), BECN1 (Santacruz H-300, sc-11427; 1:250), ATG7 (Sigma-Aldrich, A2856; 1:1,000), ULK1 (Sigma-Aldrich, A7481; 1:250), ULK3 (Sigma-Aldrich, SAB4200132; 1:500), SCD1 (Abcam, ab19862; 1:1,000), FASN (Cell Signaling, 3180; 1:1,000) and Tubulin (Millipore, 05-829; 1:5,000).

qRT-PCR. Total RNA was extracted from cells and tissues using RNeasy (Qiagen) according to the manufacturer's instructions, and treated with DNase before reverse transcription. cDNA was generated using qScript cDNA SuperMix (Quanta BioSciences). The cDNA was used as a template in real-time quantitative PCR reactions with specific primers on an ABI 7900HT Fast Real-Time PCR System. The reactions were prepared using SyBR Green reaction mix from Roche. The gene (*RPLP0*) encoding ribosomal protein P0 (RPP0) was used as a control for normalization. Human primer sequences for qRT-PCR: *RPLP0*-fw, 5'-TTCATTGTGGGAGCAGAC-3'; *RPLP0*-rev, 5'-CAGCAGTTTCTCCAGAGC-3'; *NR1D1*-fw, 5'-GCATGGAGAATCCGCTTC-3'; *NR1D1*-rev, 5'-CGGTTCTTCAGCACAGAG-3'; *NR1D2*-fw, 5'-CATTCTATATTTGAAAGTAGCCCAAT-3'; *NR1D2*-rev, 5'-ACTCAATCAAAGAATGTGCTGTGAA-3'; *ULK2*-fw, 5'-TCAAGCATCTTCCAACCTGTT-3'; *ULK2*-rev, 5'-ATTC CCGTGGCTCATTCCAT-3'; *LKB1*-fw, 5'-GAGCTGATGTCGGTGGGTATG-3'; *LKB1*-rev, 5'-CACCTTGCCGTAAGAGCCT-3'; *ULK1*-fw, 5'-AAGCAGC ATTTGGAGGTCGC-3'; *ULK1*-rev, 5'-TGATTTCTTCCCCAGCAGC-3'; *BECN1*-fw, 5'-CCATGCAGGTGAGCTTCGT-3'; *BECN1*-rev, 5'-GAATCTG CAGAGACACCATC-3'; *ULK3*-fw, 5'-TGAAGGAGCAGGTCAAGATGA-3'; *ULK3*-rev, 5'-GCTACGAACAGATTCGACAG-3'; *CDKN2B*-fw, 5'-GCGGG GACTAGTGGAGAAG-3'; *CDKN2B*-rev, 5'-CTGCCCATCATCATGACCT-3'; *CDKN2A*-fw, 5'-CCCAACGCACCGAATAGTTAC-3'; *CDKN2A*-rev, ATTCCA ATTTCCCTGCAAACT-3'; *SCD1*-fw, 5'-GACGATGAGCTCTGCTGTT-3'; *SCD1*-rev, 5'-CTCTGCTACACTTGGAGCC-3'; *FASN*-fw, 5'-CATCGGCTCC ACCAAGTC-3'; *FASN*-rev, 5'-GCTATGGAAGTGCAGGTTGG-3'; Mouse primer sequences for qRT-PCR: *ulk1*-fw, 5'-GAGCCGAGAGTGGGGCTTTGC-3'; *ulk1*-rev, 5'-GCCCTGGCAGGATACCACGC-3'; *atg7*-fw, 5'-CCGGTGGCTTCC TACTGTTA-3'; *atg7*-rev, 5'-AAGGCAGCGTTGATGACC-3'.

Chromatin immunoprecipitation with sequencing data analysis. Peak calling was performed using model-based analysis of chromatin immunoprecipitation with sequencing (ChIP-seq) (MACS)³⁵ with Galaxy Tool Version 1.0.1³⁵. *P*-value cutoff for peak detection was selected as $\leq 10^{-5}$, and the false discovery rate as ≤ 0.05 . **Promoter motif analysis.** Regions that are 2,000 bp upstream and 100 bp downstream from the transcription start sites of *Becn1*, *Atg7*, *Ulk1* and *Ulk3* were scanned using the mouse (mm10) genome annotation using the HOMER v4.9.1 findMotifs.pl script with start = -2,000 and end = 100 and a log odds-score threshold of 5, looking for the motif 'GTAGGTCCTGGGTC' and trained on data from a previous study³⁶.

Lipid extraction. Lipid extraction was performed as previously described^{37,38}. A172 cells were vortexed for 30 s in a mixture of 1:1:2 PBS:methanol:chloroform. A ¹³C₁₆-palmitic acid standard (200 pmol per sample) was added to chloroform before extraction. The resulting mixture was centrifuged at 2,200 g, 5 min, 4°C to separate organic and aqueous phases. The organic phase (bottom layer) was collected and dried under a stream of nitrogen.

Lipidomic analysis. Lipidomic analysis was performed as previously described³⁹. In brief, a Bio-Bond 5U C4 column (Dikma) was used to achieve separation of lipids. The liquid chromatography solvents were as follows: buffer A, 95:5 H₂O:methanol + 0.03% NH₄OH; buffer B, 60:35:5 isopropanol:methanol:H₂O + 0.03% NH₄OH. A typical liquid chromatography run consisted of the following for 70 min after injection: 0.1 ml min⁻¹ 100% buffer A for 5 min, 0.4 ml min⁻¹ linear gradient from 20% buffer B to 100% buffer B over 50 min, 0.5 ml min⁻¹ 100% buffer B for 8 min and equilibration with 0.5 ml min⁻¹ 100% buffer A for 7 min. Lipidomic analysis was performed using a Thermo Fisher Scientific Q Exactive Plus fitted with a heated electrospray ionization source in negative ionization mode. The MS source parameters were 4-kV spray voltage, with a probe temperature of 437.5°C and capillary temperature of 268.75°C. Full-scan mass spectrometry data was collected at a resolution of 70k, automatic gain control target 1 $\times 10^6$, maximum injection time of 100 ms and a scan range of 150–2,000 *m/z*. Data-dependent mass spectrometry (top 5 mode) was acquired

at a resolution of 35k, automatic gain control target 1×10^5 , maximum injection time of 50 ms, isolation window 1 *m/z*, scan range 200–2,000 *m/z* and a stepped normalized collision energy of 20, 30 and 40. Extracted ion chromatograms for each lipid were generated using a threshold of 5 p.p.m. around the molecular anion $[M-H]^-$ exact mass. Lipids, acyl chain composition and degree of unsaturation were validated by analysing the product ions in the corresponding tandem mass spectra. Relative quantification of lipids was performed by measuring the area under the peak and dividing this number by the area under the peak for the internal standard $^{13}C_{16}$ -palmitic acid.

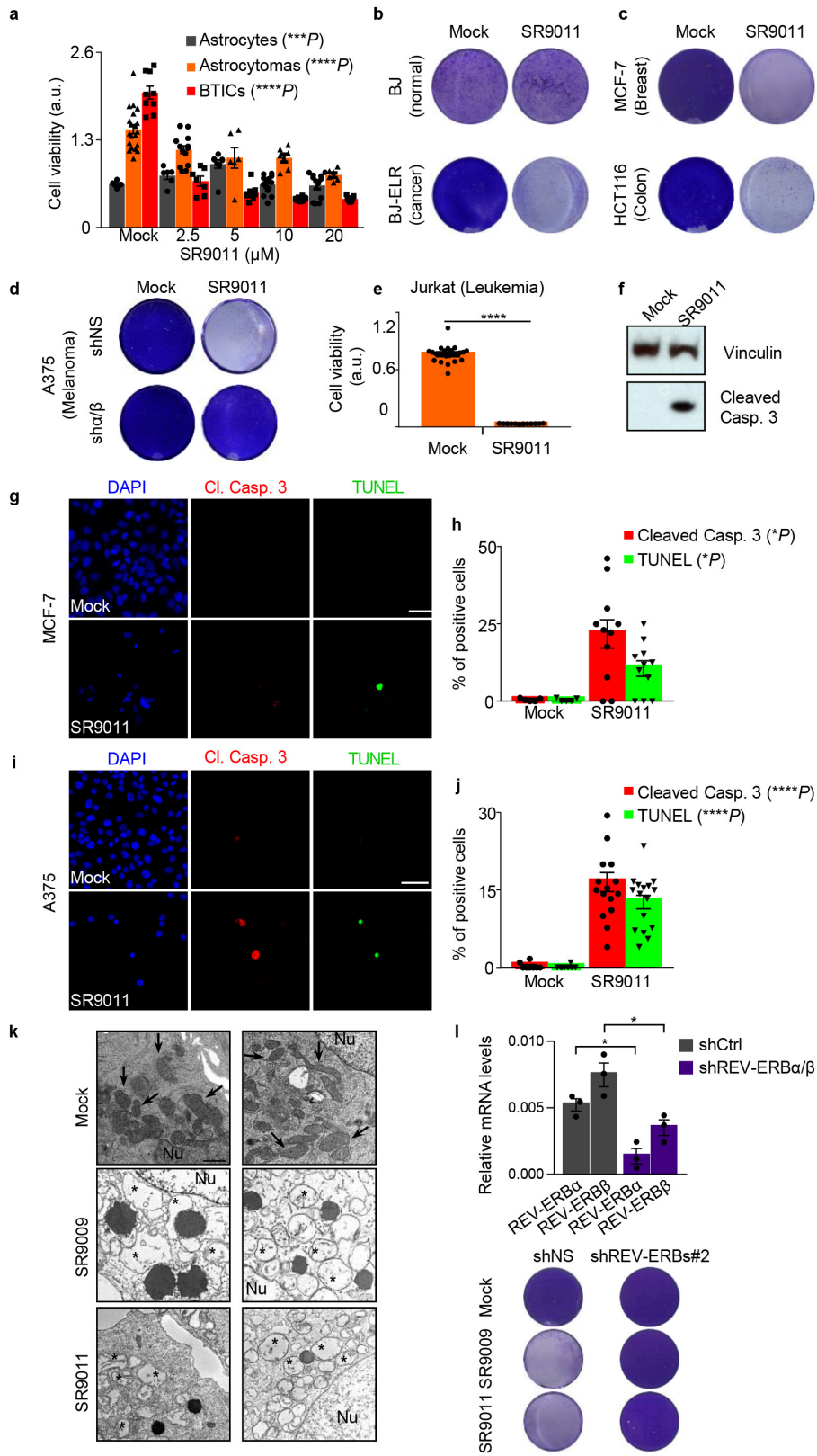
In vivo experiments. Mice were purchased from The Jackson Laboratories. All the colonies were bred as indicated by Jackson Laboratories and maintained in pathogen-free conditions at The Salk Institute, except NOD.Cg-Prkdc^{scid}Il2rg^{tm1Wjl}/SzJ mice, which were maintained at The University of Texas MD Anderson Cancer Center and Tyr-Nras^{Q61K} mice and their wild-type counterparts, which were maintained at the University of California, Irvine. C57BL/6J, NOD.Cg-Prkdc^{scid}Il2rg^{tm1Wjl}/SzJ and Tyr-Nras^{Q61K} 3–14-week-old male and female mice were used. No statistical methods were used to predetermine sample size but it was determined according to previous experimental observations. All the procedures performed in this study were approved by the Institutional Animal Care and Use Committee of the SALK institute, the University of California, Irvine and the University of Texas MD Anderson Cancer Center. In all experiments, mice were monitored daily for signs of illness and were euthanized when they reached endpoints. The 005 cells (5×10^4 cells per 1.5 μ l) or GSC 8.11 cells (1.5×10^5 per 1.5 μ l) were stereotaxically injected into anaesthetized 8–16-week-old mice (C57BL/6J for 005 cells, and NOD.Cg-Prkdc^{scid}Il2rg^{tm1Wjl}/SzJ for GSCs). The following coordinates were used: subventricular zone, 1.5 mm, 2.0 mm and 2.3 mm; hard palate, 2.0 mm, 1.5 mm and 2.3 mm; cerebral cortex, 1 mm, 1 mm, and 0.5 mm or 1.0 mm; 0 mm, 1 mm and 0.5 mm or 1.0 mm; and 2.0 mm, 1.5 mm and 0.5 mm; striatum, 0 mm, 1.4 mm and 3.0 mm (all measurements are posterior, lateral and dorsal to the bregma, respectively). To ensure that each experimental group had an equivalent starting tumour, after tumour sizes were quantified by magnetic resonance imaging mice were divided into two groups (vehicle and SR9009) and three weeks after injection, the treatment was started. Similarly, NOD.Cg-Prkdc^{scid}Il2rg^{tm1Wjl}/SzJ mice were imaged by bioluminescence imaging and after tumour sizes were quantified they were divided in two (vehicle and SR9009) or three groups (vehicle, SR9009 and temozolomide). The experiments were not randomized and investigators were not blinded to allocation during experiments and outcome assessment.

For all bioluminescence imaging, D-luciferin (150 mg kg^{-1}) was administered by subcutaneous injection to mice 10 min before imaging. Mice were fed with Picolab Diet 20 No. 5058. SR9009 was administered twice per day by intraperitoneal injection at the indicated concentrations for one week, and on subsequent days once a day unless otherwise stated. Temozolomide was administered once per day by intraperitoneal injection at 82.5 mg kg^{-1} for 5 days. All mice in this study were kept according to guidelines approved by the Animal Care and Use Committee of the Salk Institute. For the naevi studies, both ears of Tyr-Nras^{Q61K} and wild-type littermate mice at postnatal day 21 were treated with SR9009 or DMSO. Forty microlitres of drug SR9009 at $20 \mu\text{M}$ diluted with DMSO was applied to each ear twice daily for twelve consecutive days. Mice were killed one hour after the final treatment. Four mice (eight ears) were used in each group.

Statistical analysis. Results are shown as means \pm s.d. or s.e.m., as indicated in the figure legends. *P* values were calculated as indicated in figure legends, with 95% confidence level.

Data availability. All data and reagents are available from the authors upon reasonable request. All gel source data are available in Supplementary Fig. 1. Tumour source data (Fig. 4f and Extended Data Fig. 9d, i) are available as Source Data; ChIP-seq data⁵ and The Cancer Genome Atlas data^{30,31} have previously been published.

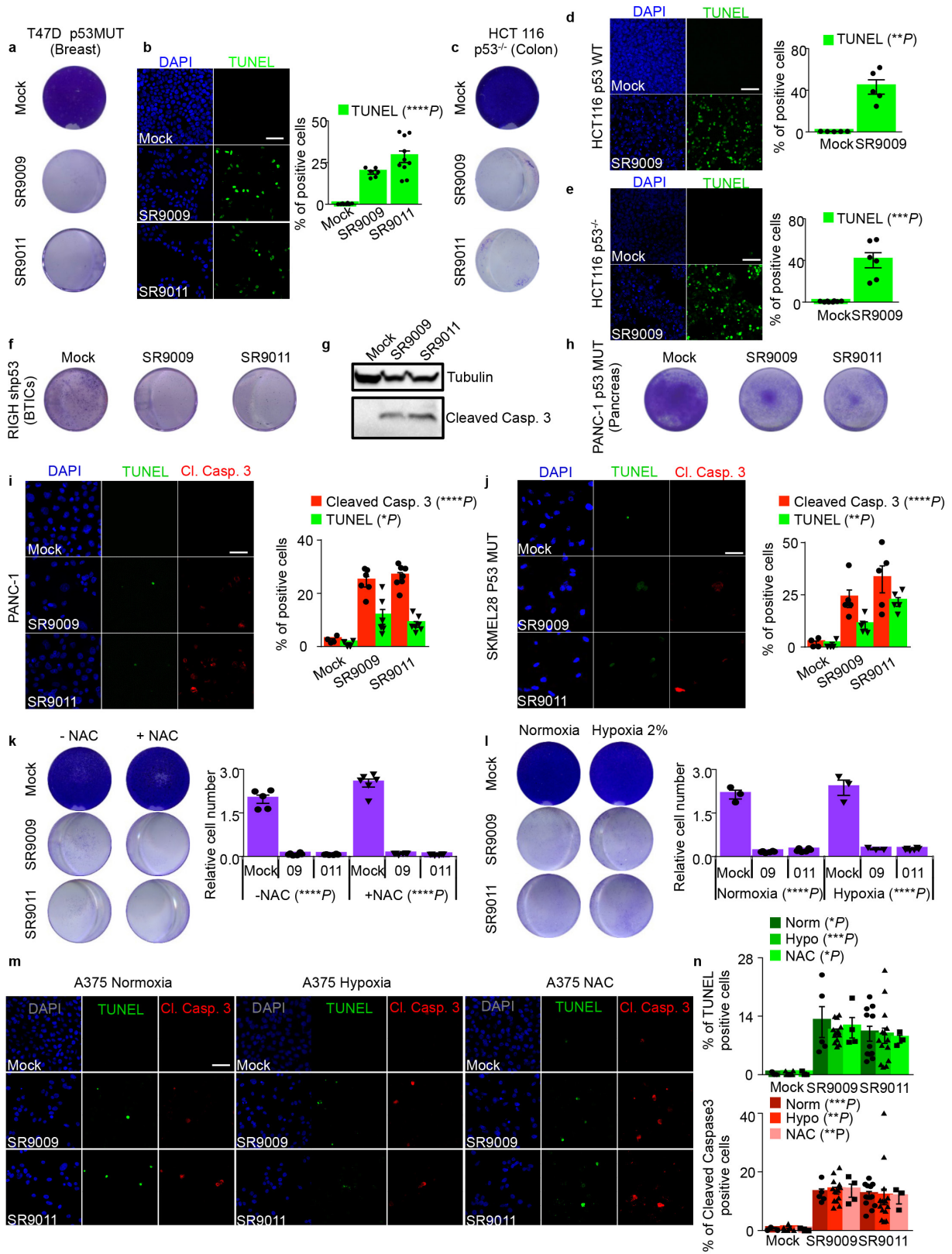
32. Marumoto, T. *et al.* Development of a novel mouse glioma model using lentiviral vectors. *Nat. Med.* **15**, 110–116 (2009).
33. Di Micco, R. *et al.* Interplay between oncogene-induced DNA damage response and heterochromatin in senescence and cancer. *Nat. Cell Biol.* **13**, 292–302 (2011).
34. Hossain, A. *et al.* Mesenchymal stem cells isolated from human gliomas increase proliferation and maintain stemness of glioma stem cells through the IL-6/gp130/STAT3 pathway. *Stem Cells* **33**, 2400–2415 (2015).
35. Zhang, Y. *et al.* Model-based analysis of ChIP-seq (MACS). *Genome Biol.* **9**, R137 (2008).
36. Lam, M. T. *et al.* Rev-Erbs repress macrophage gene expression by inhibiting enhancer-directed transcription. *Nature* **498**, 511–515 (2013).
37. Bligh, E. G. & Dyer, W. J. A rapid method of total lipid extraction and purification. *Can. J. Biochem. Physiol.* **37**, 911–917 (1959).
38. Saghatelian, A. *et al.* Assignment of endogenous substrates to enzymes by global metabolite profiling. *Biochemistry* **43**, 14332–14339 (2004).
39. Svensson, R. U. *et al.* Inhibition of acetyl-CoA carboxylase suppresses fatty acid synthesis and tumor growth of non-small-cell lung cancer in preclinical models. *Nat. Med.* **22**, 1108–1119 (2016).



Extended Data Figure 1 | See next page for caption.

Extended Data Figure 1 | SR9011, an additional agonist of REV-ERBs, selectively kills cancer cell lines. **a**, Viability assay shows that SR9011 is cytotoxic specifically in cancer cells (72 h). One-way ANOVA. *n* indicates biological replicates: astrocytes, *n* = 7 (mock), *n* = 7 (2.5 μ M), *n* = 9 (5 μ M), *n* = 13 (10 μ M) and *n* = 13 (20 μ M), $***P = 0.0004$; astrocytomas, *n* = 21 (mock), *n* = 15 (2.5 μ M), *n* = 7 (5 μ M), *n* = 8, (10 μ M), *n* = 7 (20 μ M), $****P < 0.0001$; BTICs, *n* = 10 (mock), *n* = 8 (2.5 μ M), *n* = 9 (5 μ M), *n* = 13 (10 μ M), *n* = 10 (20 μ M), $****P < 0.0001$. **b–d**, Proliferation assay showing that SR9011 treatment does not affect normal BJ cells, but is deleterious for transformed BJ-ELR cells and the cancer cell lines MCF-7 and HCT116 (20 μ M, 7 days). Depletion of REV-ERBs by shRNA impairs apoptosis induction by the SR9011 agonist of REV-ERBs; *n* = 3 biologically independent experiments. **e**, Human acute T-cell leukaemia cells are affected by the SR9011 agonist of REV-ERBs (72 h, one-tailed Mann–Whitney test, $****P < 0.0001$; *n* = 24 (mock) and 12 (SR9011) biological replicates). **f**, Immunoblot analysis of cleaved caspase 3 shows that agonists of REV-ERBs trigger apoptosis in the A375 melanoma cell line (representative of *n* = 2 biologically independent experiments).

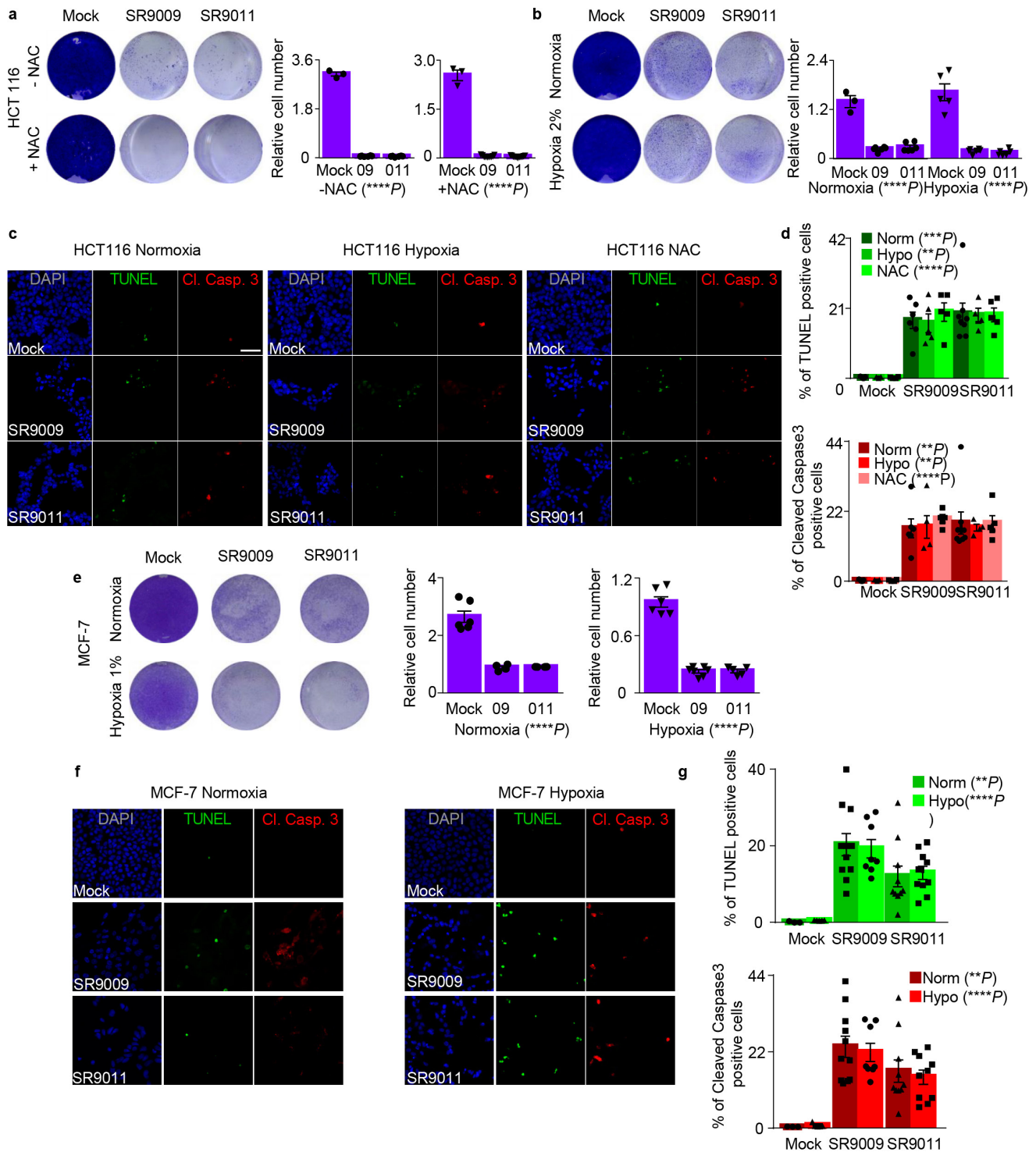
g–j, Immunostaining for cleaved caspase 3 and TUNEL assay confirm apoptosis induction by SR9011 in the cancer cell lines MCF-7 and A375. **h, j**, quantification of **g** and **i**, respectively. *n* indicates biologically independent samples; MCF-7, *n* = 5 (mock) or 11 (SR9011); A375, *n* = 8 (mock) or 16 (SR9011). One-tailed Mann–Whitney test, MCF-7 cleaved caspase 3, $*P = 0.0117$; TUNEL assay, $*P = 0.0231$; A375 cleaved caspase 3, $****P < 0.0001$; TUNEL assay, $****P < 0.0001$. Scale bars, 50 μ m. **k**, Electron microscopy confirms induction of apoptosis, as indicated by extensive presence of swollen mitochondria (representative of *n* = 3 biologically independent samples in two experiments). Arrows, normal mitochondria; asterisks, swollen mitochondria. Nu, nucleus. Scale bar, 1 μ m. **l**, Downregulation of *NR1D1* and *NR1D2* is confirmed by qRT-PCR (A375). *n* = 3 biologically independent samples. One-tailed Mann–Whitney test, $*P = 0.05$. All panels representative of three biologically independent experiments unless otherwise specified. All data are mean \pm s.e.m. a.u., arbitrary units. For gel source data, see Supplementary Fig. 1.



Extended Data Figure 2 | See next page for caption.

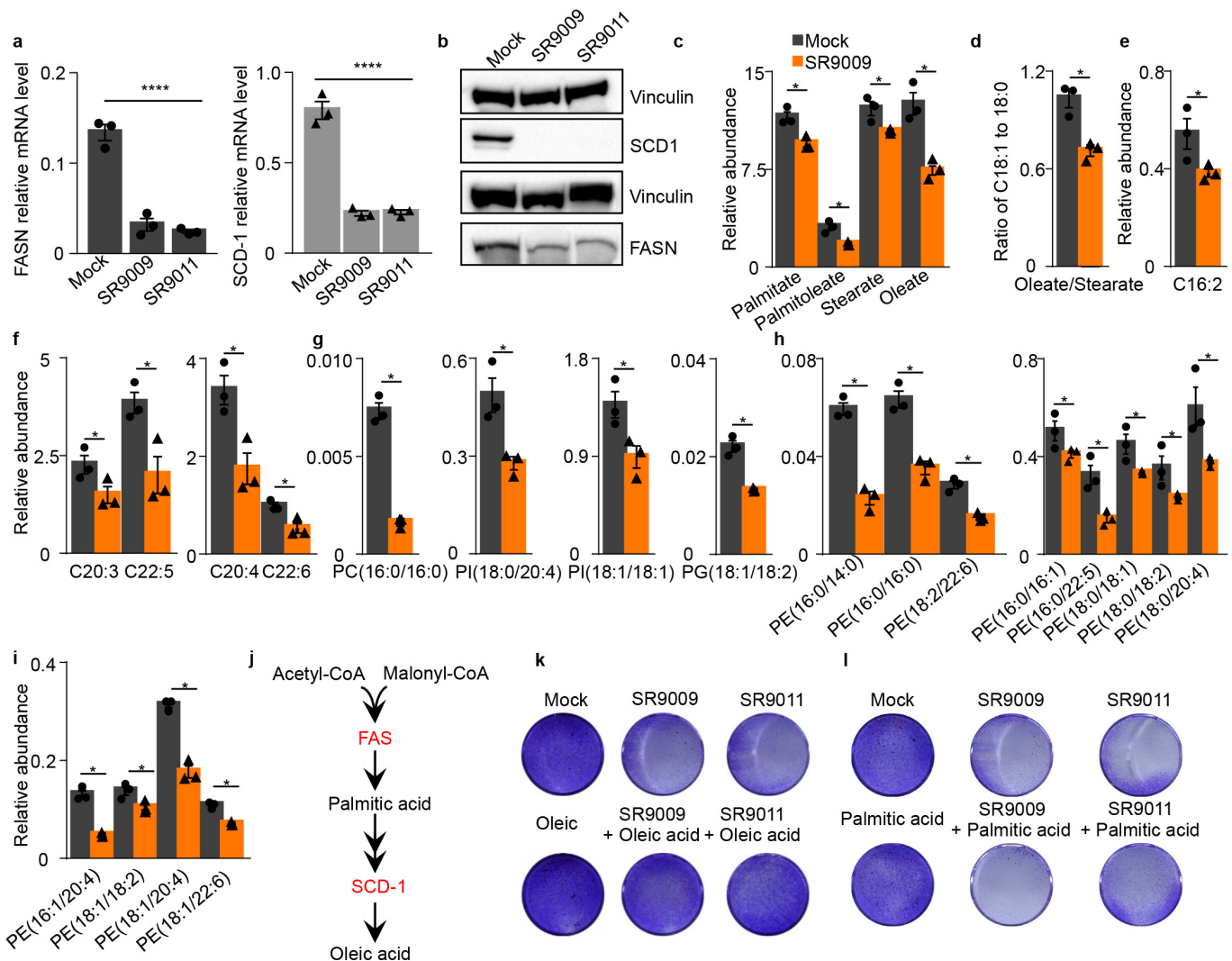
Extended Data Figure 2 | Induction of apoptosis by agonists of REV-ERBs is independent of p53 and oxidative stress. a–j. Treatment with agonists of REV-ERBs triggers apoptosis independently of p53 status, as shown by proliferation assay (7 days, 20 μ M; **a, c, f, h**) and TUNEL assay (3 days, 20 μ M; **b, i, j**) in cancer cell lines affected by various types of p53 alteration. *n* indicates biologically independent samples; T47D, *n* = 8 (mock), *n* = 6 (SR9009) and *n* = 10 (SR9011), one-way ANOVA, *****P* < 0.0001; PANC-1, *n* = 4 (mock), *n* = 6 (SR9009) and *n* = 7 (SR9011), one-way ANOVA; TUNEL assay, **P* = 0.0108; cleaved caspase 3, *****P* < 0.0001; SKMEL28, *n* = 4 (mock), *n* = 5 (SR9009, SR9011), one-way ANOVA; TUNEL assay, *****P* < 0.0001; cleaved caspase 3, ***P* = 0.0035. **d, e**, Apoptosis is induced in both wild-type and p53-null HCT116 cells (TUNEL assay, 4 days, 20 μ M, mean \pm s.e.m.). One-tailed Mann–Whitney test. *n* indicates biologically independent samples. HCT116 wild type, *n* = 5 (mock, SR9009), ***P* = 0.004; HCT116 p53 knockout, *n* = 8 (mock) or 6 (SR9009), ****P* = 0.0003. **f**, Immunoblot analysis of cleaved caspase 3 shows that agonists of REV-ERBs trigger apoptosis in the RIGH cell line (one experiment). **k**, Co-treatment with the reducing agent NAC (10 mM) does not rescue the viability of A375 cells

(20 μ M, 7 days). *n* indicates biological replicates, *n* = 5 (mock, –NAC) or 6 (all other dot plots). One-way ANOVA, *****P* < 0.0001. **l**, Results obtained under hypoxic conditions (20 μ M, 6 days) were similar to those obtained in co-treatments with NAC. *n* indicates biological replicates, *n* = 3 (mock –NAC, mock hypoxia and SR9009 hypoxia) or 6 (SR9009 normoxia, SR9011 normoxia and SR9011 hypoxia). One-way ANOVA, *****P* < 0.0001. **m, n**, Hypoxia or co-treatment with NAC does not alter the ability of agonists of REV-ERBs to induce apoptosis in A375 cells. One-way ANOVA. *n* indicates biologically independent samples: normoxia, *n* = 3 (mock), *n* = 5 (SR9009) or *n* = 11 (SR9011); TUNEL assay, **P* = 0.0432; cleaved caspase 3, ****P* = 0.0004; hypoxia, *n* = 6 (mock), *n* = 13 (SR9009) or *n* = 14 (SR9011); TUNEL assay, ****P* = 0.0005; cleaved caspase 3, **P* = 0.0028; NAC, *n* = 3 (mock), *n* = 4 (SR9009) or *n* = 3 (SR9011); TUNEL assay, **P* = 0.0104; cleaved caspase 3, ***P* = 0.0042. Scale bars, 50 μ m. All panels representative of three biologically independent experiments with similar results unless otherwise specified. All data are mean \pm s.e.m. Norm, normoxia; Hypo, hypoxia. For gel source data, see Supplementary Fig. 1.



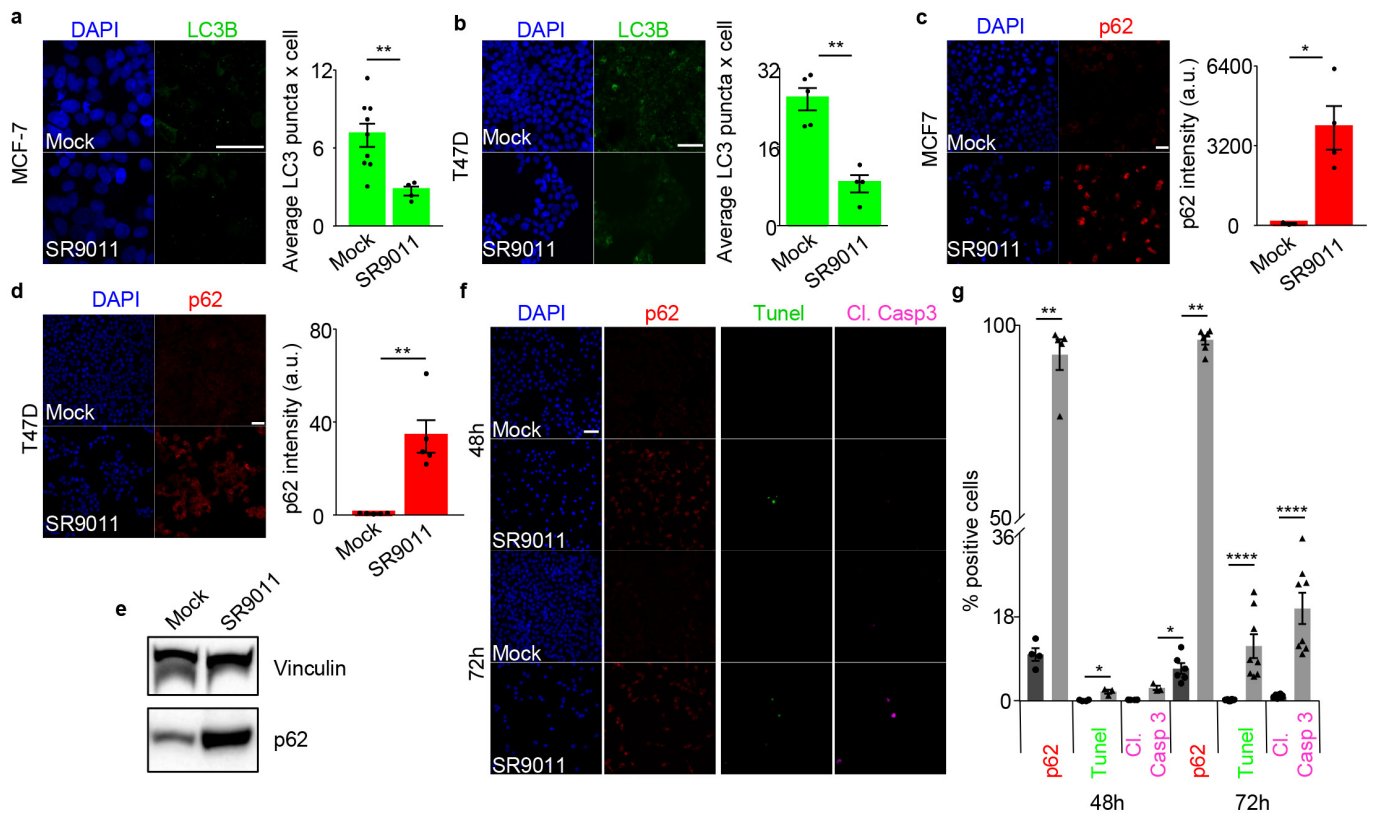
Extended Data Figure 3 | Attenuation of oxidative stress does not affect the cytotoxic activity of agonists of REV-ERBs. **a, b,** Treatment with agonists of REV-ERBs (20 μ M) induces apoptosis on co-treatment with NAC and under hypoxic conditions, as shown by proliferation assays of HCT-116 cells. *n* indicates biological replicates. *n* = 3 (mock \pm NAC), *n* = 6 (SR9009/SR9011 \pm NAC), *n* = 9 (SR9009 + NAC), *n* = 11 (SR9011 + NAC), *n* = 3 (mock normoxia), *n* = 6 (SR9009/SR9011 normoxia and hypoxia), *n* = 5 (mock hypoxia) 6 days, one-way ANOVA, *****P* < 0.0001. **c, d,** Apoptosis induction of HCT116 cells remained unchanged under hypoxia or on co-treatment with NAC; 20 μ M, 6 days, one-way ANOVA. *n* indicates biologically independent samples: normoxia, *n* = 5 (mock), *n* = 6 (SR9009), *n* = 8 (SR9011); TUNEL assay, ****P* = 0.0003; cleaved caspase 3, ***P* = 0.0021; hypoxia, *n* = 3 (mock), *n* = 5 (SR9009), *n* = 4 (SR9011); TUNEL assay, ***P* = 0.0015; cleaved caspase 3, ***P* = 0.0046; NAC, *n* = 4 (mock), *n* = 5 (SR9009), *n* = 5

(SR9011); TUNEL assay, *****P* < 0.0001; cleaved caspase 3, *****P* < 0.0001. **e,** In MCF-7 cells, apoptosis triggered by agonists of REV-ERBs is independent of oxidative state, as shown by proliferation assay (20 μ M). *n* indicates biological replicates: *n* = 6 (mock, normoxia and hypoxia), *n* = 4 (09-011 normoxia), *n* = 7 (09 hypoxia), *n* = 5 (011 hypoxia); one-way ANOVA, *****P* < 0.0001; **f, g** TUNEL assay and immunofluorescence analysis of cleaved caspase 3 confirm previous results (Extended Data Fig 3c, d). *n* indicates biologically independent samples. *n* = 3 (mock normoxia), *n* = 5 (mock hypoxia), *n* = 11 (09 normoxia), *n* = 8 (09 hypoxia), *n* = 10 (011 normoxia and hypoxia). One-way ANOVA. Normoxia, TUNEL assay, ***P* = 0.0049; cleaved caspase 3, ***P* = 0.0054; hypoxia, TUNEL assay, *****P* < 0.0001; cleaved caspase 3, *****P* < 0.0001. All panels representative of three biologically independent experiments with similar results. All data are mean \pm s.e.m. Norm, normoxia; Hypo, hypoxia.



Extended Data Figure 4 | Agonists of REV-ERBs inhibit *de novo* lipogenesis. **a, b**, Agonists of REV-ERBs downregulate *FASN* and *SCD1* mRNA, as assayed by qRT-PCR. A172 cell line 48 h, 20 μ M; *FASN* and *SCD1*, $n = 3$ biologically independent samples, **** $P < 0.0001$. *FASN* and *SCD1* protein levels (**b**) are reduced on treatment with SR9009 and SR9011. **c–i**, Agonists of REV-ERBs reduce free fatty acid concentrations, as quantified by liquid chromatography–mass spectrometry. **c**, Relative levels of free fatty acids that are the primary products of *FASN* (palmitic acid, C16:0; stearic acid, C18:0) and *SCD1* (palmitoleic acid, C16:1; oleic acid, C18:1) are lower in samples treated with SR9009 than in control samples. **d**, The unsaturation index (changes in oleate:stearate ratio) is decreased in the SR9009-treated sample, compared to mock-treated samples, owing to the large decrease in monounsaturated oleate observed in the SR9009-treated sample. **e, f**, SR9009 treatment reduces polyunsaturated fatty acids levels compared to mock-treated samples,

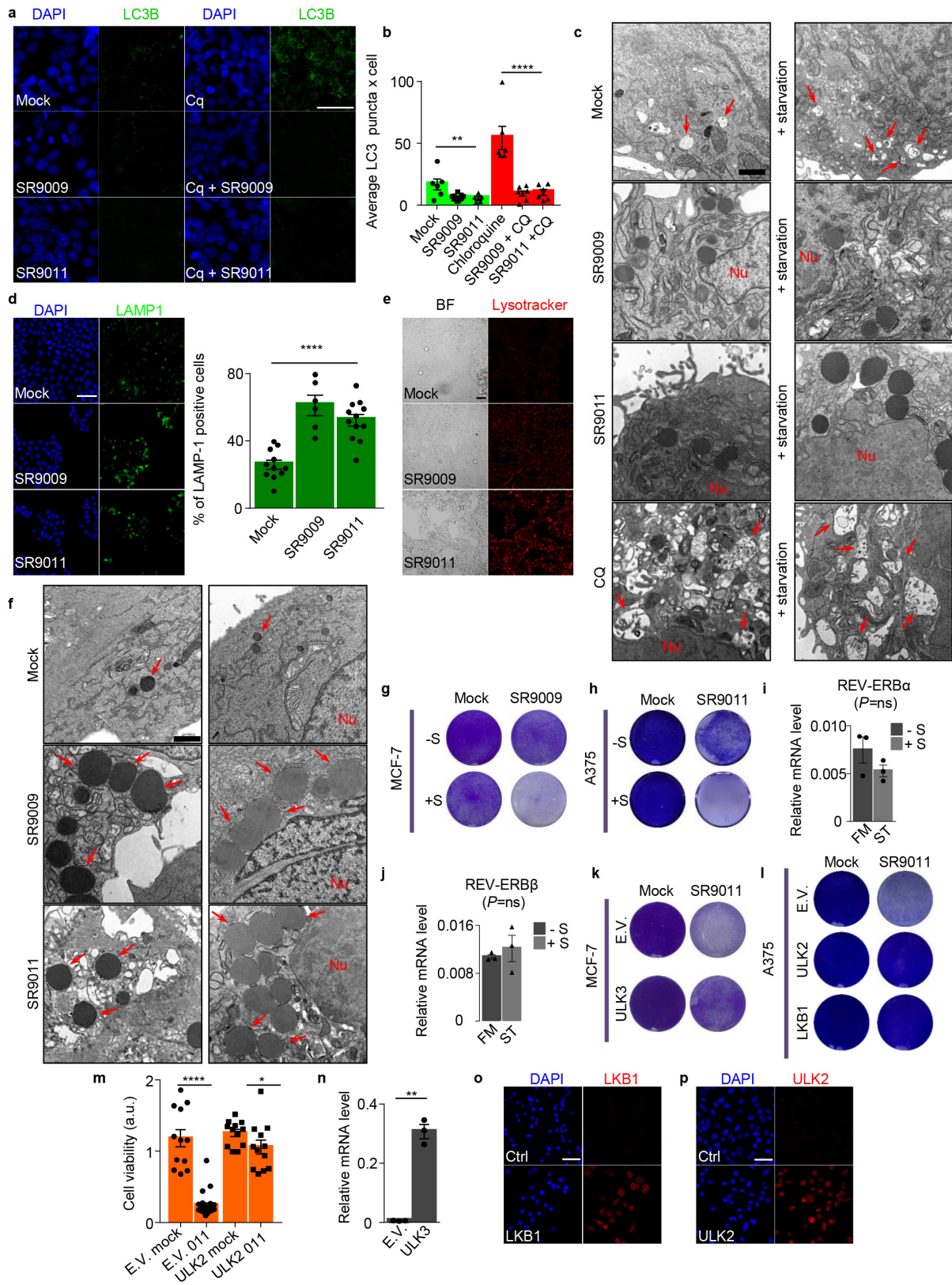
in agreement with previous results (Extended Data Fig. 3c, d). **g–i**, Decreases in free fatty acid levels can affect the concentrations of phospholipids that contain these fatty acids. Treatment with agonists of REV-ERBs leads to reductions in palmitic acid-containing phosphatidylcholine, arachidonic acid- and oleic acid-containing phosphatidylinositols, mono- and di-unsaturated phosphatidylglycerol (**g**) and phosphatidylethanolamines (**h, i**); A172 cell line 48 h, 20 μ M, * $P = 0.05$. **j**, Simplified scheme illustrating the metabolic products of *FASN* and *SCD1*. **k**, Supplementation of oleic acid partially ameliorates the cytotoxicity of agonists of REV-ERBs (A172, 20 μ M, 4 days). **l**, Supplementation of palmitic acid does not impair the cytotoxicity of agonists of REV-ERBs (20 μ M, A172, 4 days). All data are mean \pm s.e.m. P value is calculated with one-way ANOVA in panel **a**, and with one-tailed Mann–Whitney test in the remaining panels. $n = 3$ biologically independent samples (**d–i**). For gel source data, see Supplementary Fig. 1.



Extended Data Figure 5 | REV-ERB agonist SR9011 inhibit autophagy.

a, b, Treatment with SR9011 reduces the number of autophagosomes both in MCF7 and T47D cell lines. *n* indicates biologically independent samples, MCF7 20 μ M 24 h, *n* = 9 (mock), *n* = 4 (SR9011), ***P* = 0.0056; T47D 48 h 20 μ M, *n* = 5 (mock), *n* = 4 (SR9011), ***P* = 0.0079. **c, d**, SR9011 induces accumulation of p62, as shown by immunofluorescence both in MCF7 and T47D cell lines. *n* indicates biologically independent samples. MCF7 p62 48 h, *n* = 3 (mock), *n* = 4 (SR9011), **P* = 0.0286; T47D 48 h, *n* = 5 (mock and SR9011), ***P* = 0.004. **e**, Accumulation of p62 is confirmed by immunoblot (48h, 20 μ M A375). **f, g**, Inhibition of autophagy precedes

apoptosis induction, as shown by immunofluorescence of p62, cleaved caspase 3 and TUNEL assay. *n* indicates biologically independent samples: *n* = 4 (mock, 48 h), *n* = 5 (SR9011 p62), *n* = 3 (SR9011, 48 h), *n* = 6 (mock, SR9011 72 h, p62), *n* = 10 (mock, 72 h), *n* = 8 (SR9011, 72 h) A375 20 μ M; cleaved caspase 3, 48 h, **P* = 0.0286; cleaved caspase 3, 72 h, *****P* < 0.0001; TUNEL assay, 48 h, **P* = 0.0286; TUNEL assay, 72 h, *****P* < 0.0001; p62, 48 h, ***P* = 0.0079; p62, 72 h, ***P* = 0.0011. All panels representative of three biologically independent experiments with similar results. All data are mean \pm s.e.m. *P* value is calculated with one-tailed Mann-Whitney test in all panels. For gel source data, see Supplementary Fig. 1.

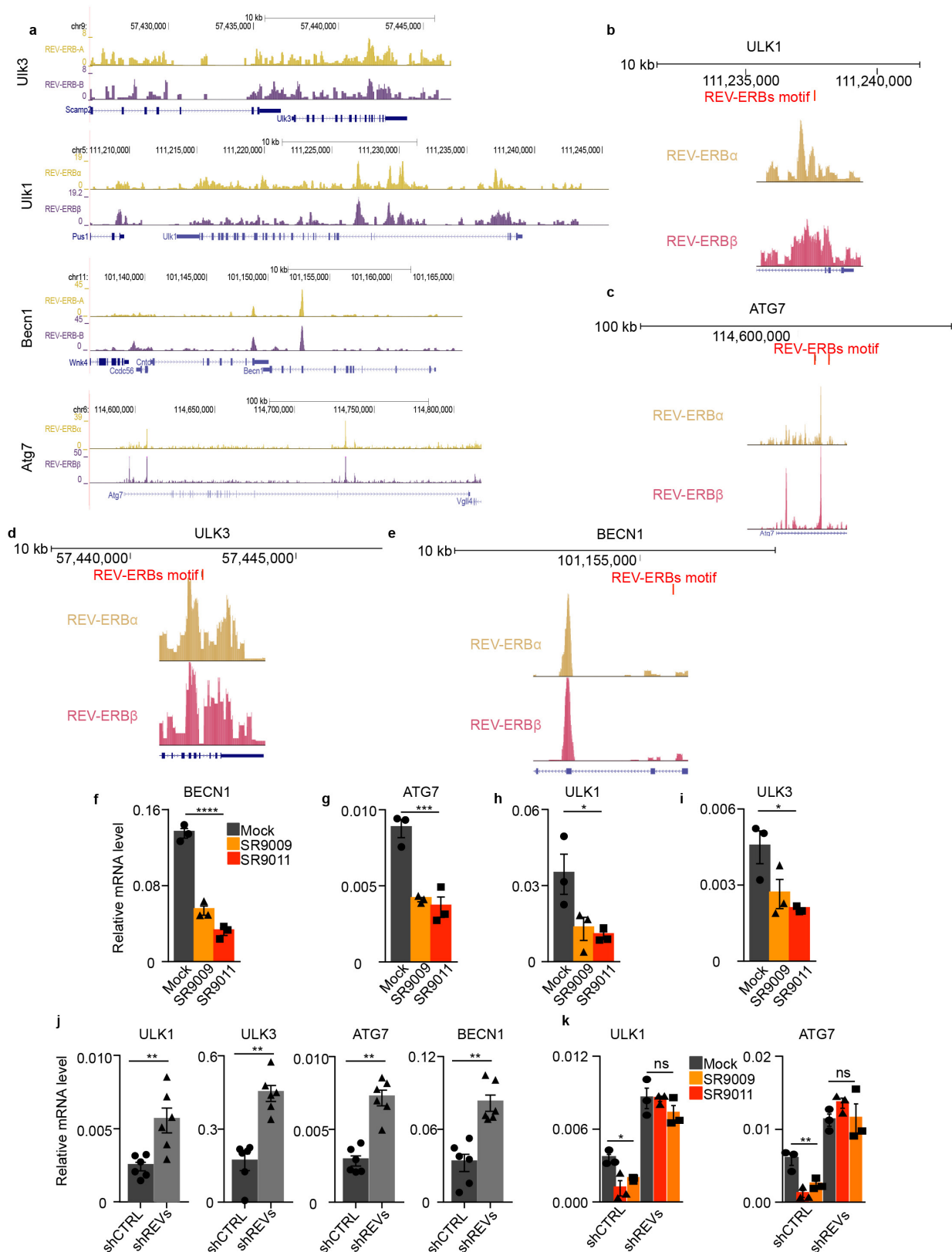


Extended Data Figure 6 | See next page for caption.

Extended Data Figure 6 | Agonists of REV-ERBs (SR9009 and SR9011)

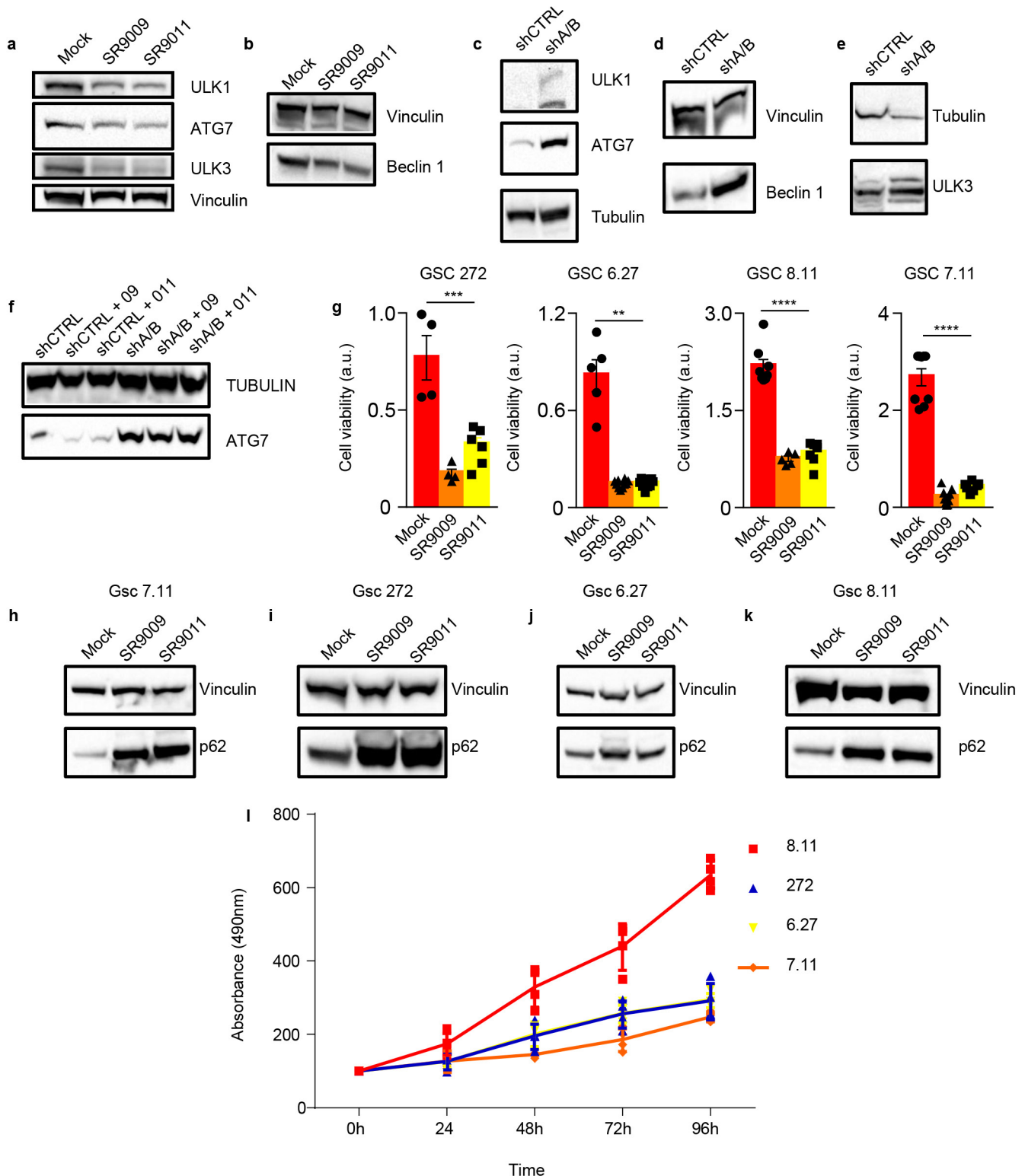
block autophagy. **a**, Agonists of REV-ERBs block autophagy, which results in reduced autophagic flux. **b**, Quantification of LC3 puncta. *n* indicates biologically independent samples. *n* = 6 (mock, chloroquine (CQ) ± SR9011), *n* = 11 (SR9009), *n* = 5 (SR9011), *n* = 7 (CQ + SR9009). One-way ANOVA: mock versus SR9009 and SR9011, ***P* = 0.0049; CQ versus CQ + SR9009 or CQ + SR9011, *****P* < 0.0001. **c**, On treatment with SR9009 and SR9011, autophagy blockage can be observed by electron microscopy, even under starvation conditions. Arrows, representative autophagosomes; Nu, nucleus. Scale bars, 1 μM. *n* = 3 biologically independent samples of two independent experiments with similar results (mock ± SR9009 and SR9011) or one experiment (mock, SR9009 and SR9011 ± starvation). **d**, Agonists of REV-ERBs induce lysosome accumulation, as shown by immunofluorescence assay for the lysosome marker LAMP1. *n* indicates biologically independent samples: *n* = 11 (mock), *n* = 6 (SR9009), *n* = 12 (SR9011). T47D, 72 h 20 μM, one-way ANOVA, *****P* < 0.0001. **e**, Lysosome accumulation is confirmed by LysoTracker Red (MCF-7, 72 h 20 μM). Scale bars, 50 μm. BF, bright field. **f**, Marked lysosomal turnover defects are revealed

with electron microscopy. *n* = 3 biologically independent samples of two independent experiments with similar results. Arrows, lysosomes; Nu, nucleus. Scale bars, 1 μM. **g, h**, Starvation synergizes with treatment with the SR9009 agonist of REV-ERBs (MCF-7 48 h, 20 μM; A375, 3 days, 20 μM). **i, j**, Starvation has no effect on expression of REV-ERBs, as shown by qRT-PCR; two-tailed Mann-Whitney test. ns, not significant; FM, fresh medium; ST, starvation. **k, l**, Overexpression of ULK3, ULK2 and LKB1 impairs the induction of apoptosis by SR9011 (MCF-7, A375 6 days, 20 μM). **m**, WST-1 viability assay shows abrogation of apoptosis in cells that overexpress ULK2. *n* indicates biological replicates: *n* = 12 (empty vector (E.V.) mock, ULK2 mock, ULK2 SR9011), *n* = 27 (E.V. SR9011) A375, 6 days, 20 μM. One-tailed Mann-Whitney test, E.V. mock versus E.V. 011, *****P* < 0.0001; ULK2 mock versus ULK2 011 **P* = 0.0225). **n**, qRT-PCR shows overexpression of ULK3 (one-tailed Student's *t*-test, ***P* = 0.0031). **o, p**, Immunofluorescence assay confirms overexpression of LKB1 and ULK2. *n* = 3 biologically independent samples (**i, j, n**). Scale bars, 50 μm. All panels representative of three biologically independent experiments with similar results, unless otherwise specified. All data are mean ± s.e.m.



Extended Data Figure 7 | Core autophagy genes are novel REV-ERBs targets. **a**, Analyses of available ChIP-seq data⁵ indicate that REV-ERBs peaks are present in *Ulk3*, *Ulk1*, *Becn1* and *Atg7* ($P < 0.00001$ calculated by MACS using Poisson distribution, false discovery rate ≤ 0.05). **b–e**, Analysis of REV-ERBs-binding motif performed using HOMER indicates the presence of REV-ERBs-binding sites in *Ulk3*, *Ulk1*, *Becn1* and *Atg7* genes (mouse genome). **f–i**, Treatment with agonists of REV-ERBs leads to downregulation of autophagy central regulators (MCF-7 72 h 20 μ M; one-way ANOVA, **** $P < 0.0001$). **j**, Autophagy genes are

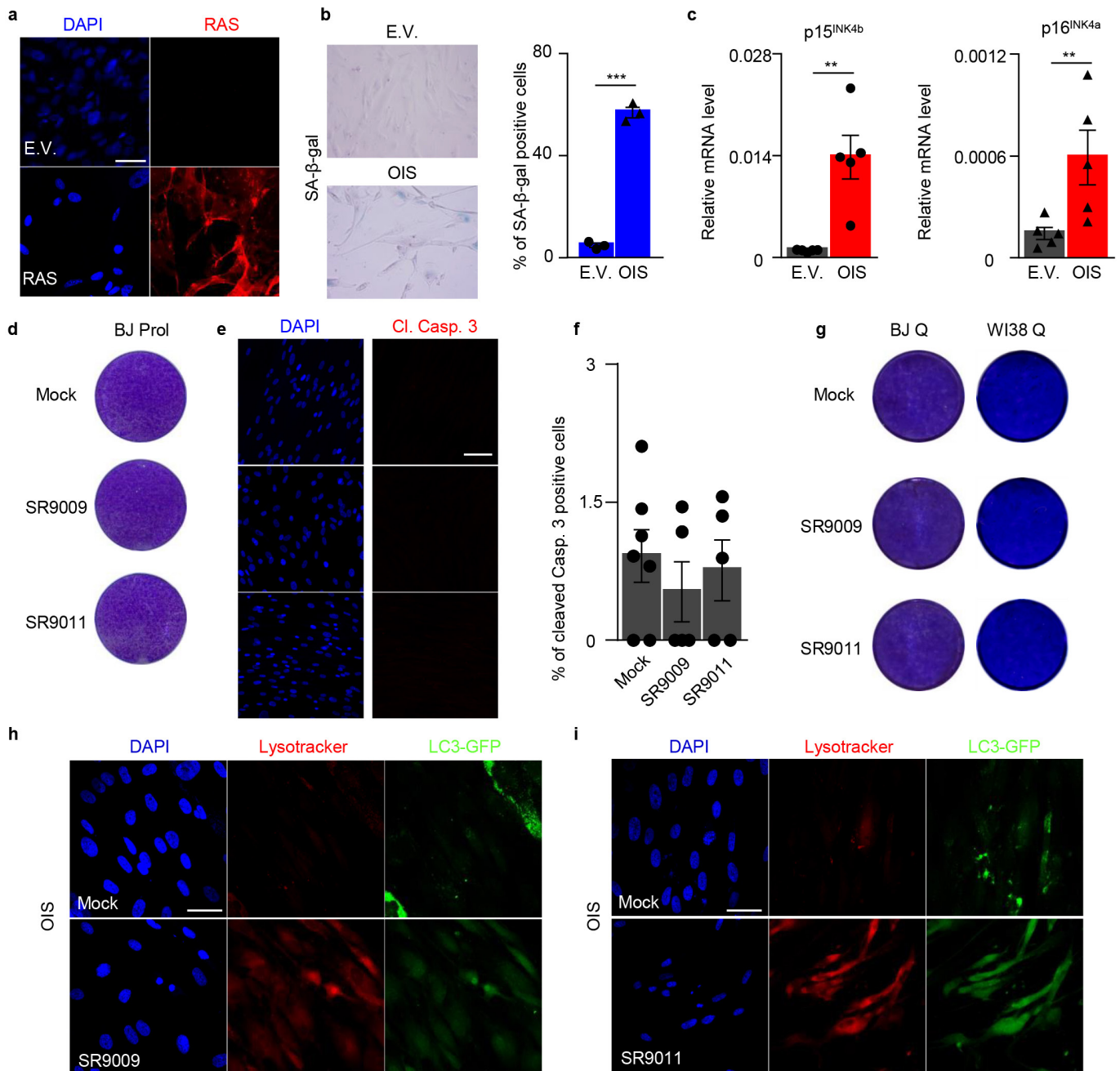
upregulated on expression of REV-ERBs shRNA. A375 cell line, $n = 6$ biologically independent samples. One-tailed Mann–Whitney test; *ULK3*, *** $P = 0.0011$; *ATG7* and *BECN1*, ** $P = 0.0011$; *ULK1*, ** $P = 0.0043$. **k**, The repression of autophagy genes caused by SR9009 and SR9011 is abrogated in A375 cells expressing REV-ERBs shRNA; control shRNA \pm SR9009 or SR9011, one-way ANOVA; *ULK1*, * $P = 0.0162$; *ATG7*, ** $P = 0.0036$. **f–i**, **k**, $n = 3$ biologically independent samples. All data are mean \pm s.e.m. shREVs, shNR1D1 and shNR1D2; shCTRL, non-silencing shRNA.



Extended Data Figure 8 | REV-ERBs regulate autophagy core genes and block autophagy in slowly proliferating cancer stem cells.

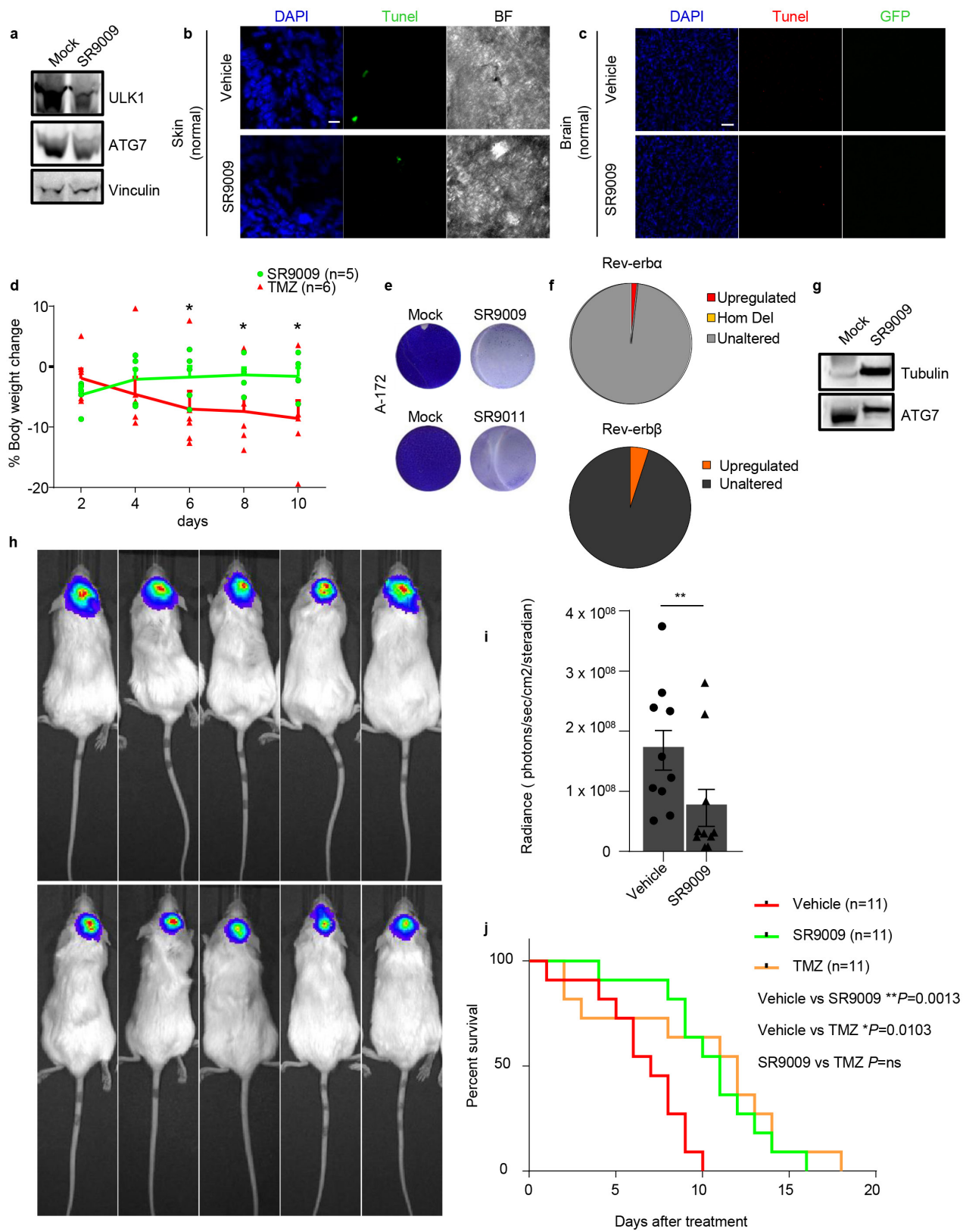
a, b, Immunoblot analyses show a reduction of ULK1, ATG7, ULK3 and BECN1 protein levels on treatment with agonists of REV-ERBs (MCF-7 72 h 20 μ M). **c–e**, REV-ERBs shRNA increases protein levels of autophagy regulators (A375). **f**, The reduction in ATG7 protein levels on treatment with SR9009 and SR9011 is abrogated in cells expressing REV-ERBs shRNA. **g**, WST-1 viability assays show that treatment with SR9009 and SR9011 is cytotoxic specifically in patient-derived glioblastoma stem cells; mean \pm s.e.m., 5 days, one-way ANOVA. *n* indicates biological replicates: GSC 272, *n* = 4 (mock, SR9009), *n* = 6 (SR9011), ****P* = 0.0002;

GSC 6.27, *n* = 5 (mock), *n* = 10 (SR9009), ***P* = 0.003; GSC 8.11, *n* = 8 (mock), *n* = 5 (SR9009), *n* = 7 (SR9011), *****P* < 0.0001; GSC 7.11, *n* = 9 (mock, SR9009), *n* = 7 (SR9011), *****P* < 0.0001. **h–k**, Immunoblot analyses show accumulation of p62 in patient-derived glioblastoma stem cells (one independent experiment). **l**, MTS assays show that GSC 6.27, 7.11 and 272 are characterized by a slow proliferation rate; *n* = 4 biologically independent samples, four experiments, mean \pm s.d. All panels representative of three biologically independent experiments with similar results, unless otherwise specified. For gel source data, see Supplementary Fig. 1.



Extended Data Figure 9 | Agonists of REV-ERBs do not affect viability of normal proliferating and quiescent OIS cells. **a**, Immunofluorescence assay for RAS confirms RAS overexpression in OIS cells. **b**, SA-β-galactosidase assay shows induction of senescence; $n = 3$ biologically independent samples, one-tailed Student's t -test, **** $P < 0.0001$. **c**, Induction of cell cycle inhibitors *CDKN2B* and *CDKN2A* is assayed by qRT-PCR. $n = 5$ biologically independent samples. One-tailed Mann-Whitney test, *CDKN2B*, ** $P = 0.004$; *CDKN2A*, ** $P = 0.0079$. **d**, **e**, Agonists of REV-ERBs do not induce apoptosis in proliferating and quiescent normal diploid BJ fibroblasts (**d**–**g**), as shown by proliferation

assay (**d**, 7 days, 20 μ M) and immunofluorescence for cleaved caspase 3 (**e**, **f**, 7 days, 20 μ M). One-way ANOVA. n indicates biologically independent samples: $n = 7$ (mock), $n = 5$ (SR9009, SR9011). Cell viability is also not affected in an additional normal diploid WI38 cell line (**g**, 10 days, 20 μ M). **h**, **i**, SR9009 and SR9011 inhibit autophagy in OIS cells, as shown by the accumulation of lysosomes (LysoTracker Red) and the absence of LC3 puncta (3 days, 20 μ M). Scale bars, 50 μ m. Data in **a**–**i** are representative of three independent experiments with similar results, unless otherwise specified. All data are mean \pm s.e.m.



Extended Data Figure 10 | See next page for caption.

Extended Data Figure 10 | SR9009 impairs tumour growth and improves survival of glioblastoma patient-derived xenografts. **a**, Protein levels of autophagy genes in NRAS naevi are reduced upon treatment with SR9009, as assayed by immunoblot ($n = 4$ mice, one experiment). **b**, TUNEL assays show that apoptosis induction is absent in normal skin on treatment with SR9009 ($n = 4$ mice, one experiment, 12 days, SR9009 20 μM). Scale bar, 10 μm ; BF, bright field. **c**, TUNEL assays show that apoptosis induction is absent in normal brain tissues on treatment with SR9009 (6 days, 200 mg kg^{-1} twice a day, $n = 5$ mice, one experiment). **d**, Treatment with SR9009 (100 mg kg^{-1} twice a day) is tolerated better than temozolomide administration (82.5 mg kg^{-1} once a day for 5 days), as shown by measurement of percentage body weight change. One-tailed Mann–Whitney test; day 6, 8, 10, $*P = 0.0411$, mean \pm s.e.m. $n = 5$ (SR9009) or 6 (temozolomide) mice. **e**, The glioblastoma cell line A172 is sensitive to treatment with SR9009 and SR9011 (20 μM 6 days, three biologically independent experiments with similar results). **f**, Previous analyses³⁰ of The Cancer Genome Atlas data show genetic

alterations that affect *NR1D1* and *NR1D2* are absent. Gene expression analysis shows that no cases are present with downregulation of REV-ERBs, and only a small fraction with upregulation. $n = 574$ biologically independent samples. *NR1D1*: upregulation, 1.56%; homozygous deletion (Hom Del), 0.17%; unaltered, 98.27%. *NR1D2*: upregulation, 4.54%; unaltered, 95.46%. **g**, *In vivo* treatment with SR9009 results in the decrease of ATG7 protein levels (6 days, 200 mg kg^{-1} twice a day, $n = 5$ mice, one experiment). **h**, SR9009 treatment impairs *in vivo* growth of glioblastoma patient-derived xenografts (6 days, 200 mg kg^{-1} , $n = 5$ mice). **i**, Quantification of tumour size by *in vivo* luciferase assays (mean \pm s.e.m., $n = 10$ mice, one-tailed Mann–Whitney test, $**P = 0.0057$). **j**, SR9009 improves survival in mice that bear glioblastoma patient-derived xenografts. SR9009 200 mg kg^{-1} twice a day, $n = 11$ (vehicle), $n = 11$ (SR9009), $n = 11$ (temozolomide (82.5 mg kg^{-1} once a day for 5 days)) mice; two-tailed log-rank analyses. For gel source data, see Supplementary Fig. 1.

Life Sciences Reporting Summary

Nature Research wishes to improve the reproducibility of the work that we publish. This form is intended for publication with all accepted life science papers and provides structure for consistency and transparency in reporting. Every life science submission will use this form; some list items might not apply to an individual manuscript, but all fields must be completed for clarity.

For further information on the points included in this form, see [Reporting Life Sciences Research](#). For further information on Nature Research policies, including our [data availability policy](#), see [Authors & Referees](#) and the [Editorial Policy Checklist](#).

► Experimental design

1. Sample size

Describe how sample size was determined.

Sample size was determined according to previous experimental observations

2. Data exclusions

Describe any data exclusions.

No data were excluded

3. Replication

Describe whether the experimental findings were reliably reproduced.

Yes the experimental findings were reliably reproduced as described in the figure legends

4. Randomization

Describe how samples/organisms/participants were allocated into experimental groups.

In order to ensure that each experimental group had an equivalent starting tumor size either MRI or in vivo BLI were used in order to separate the mice into the experimental groups before treatment. No reasons to randomize experiments for this study

5. Blinding

Describe whether the investigators were blinded to group allocation during data collection and/or analysis.

No blinding

Note: all studies involving animals and/or human research participants must disclose whether blinding and randomization were used.

6. Statistical parameters

For all figures and tables that use statistical methods, confirm that the following items are present in relevant figure legends (or in the Methods section if additional space is needed).

n/a Confirmed

- The exact sample size (n) for each experimental group/condition, given as a discrete number and unit of measurement (animals, litters, cultures, etc.)
- A description of how samples were collected, noting whether measurements were taken from distinct samples or whether the same sample was measured repeatedly
- A statement indicating how many times each experiment was replicated
- The statistical test(s) used and whether they are one- or two-sided (note: only common tests should be described solely by name; more complex techniques should be described in the Methods section)
- A description of any assumptions or corrections, such as an adjustment for multiple comparisons
- The test results (e.g. P values) given as exact values whenever possible and with confidence intervals noted
- A clear description of statistics including central tendency (e.g. median, mean) and variation (e.g. standard deviation, interquartile range)
- Clearly defined error bars

See the web collection on [statistics for biologists](#) for further resources and guidance.

► Software

Policy information about [availability of computer code](#)

7. Software

Describe the software used to analyze the data in this study.

IMAGE J, SKYLINE (PMID 22454539), HOMER v4.9.1, Prism 7

For manuscripts utilizing custom algorithms or software that are central to the paper but not yet described in the published literature, software must be made available to editors and reviewers upon request. We strongly encourage code deposition in a community repository (e.g. GitHub). [Nature Methods guidance for providing algorithms and software for publication](#) provides further information on this topic.

► Materials and reagents

Policy information about [availability of materials](#)

8. Materials availability

Indicate whether there are restrictions on availability of unique materials or if these materials are only available for distribution by a for-profit company.

No restriction

9. Antibodies

Describe the antibodies used and how they were validated for use in the system under study (i.e. assay and species).

Anti-Cleaved Caspase 3, Cell signaling #9664, PubMed Id27353360; anti-vinculin clone hVIN-1 SIGMA#V9131, PubMed Id 24769727; anti Sqstm1/p62 Abcam ab56416, PubMed Id 26102349; Lc3b Cell Signaling #3868 PubMed Id 27074587; ULK2 E-19 sc-10907 PubMed Id 26920049; Lamp1 Cell Signaling #9091 PubMed Id 27278822; LKB1 Cell Signaling #13031, PubMed Id 25115923; Sqstm1/p62 MBL PM045 PubMed Id 18083104; Ras BD #610002 PubMed Id 26173259. BECN1 (1:250, Santacruz H-300, sc-11427) PMID: 26649942, ATG7 (1:1000 554 Sigma; Cat#: A2856), PMID 15866887, PMID 24721646, ULK1 (1:250, SIGMA; Cat#: A7481) PMID 21897364, PMID 25723488, ULK3 (1:500 SIGMA; Cat#: 555 SAB4200132) PMID 19279323, SCD1 (1:1000, ABCAM, ab19862), PMID: 28474697, FASN (1:1000, Cell Signaling, 556 #3180), PMID: 28099419, TUBULIN (1:5000, MILLIPORE #05-829), PMID: 25266063. We selected antibodies that have been used by experts in the fields

10. Eukaryotic cell lines

a. State the source of each eukaryotic cell line used.

BJ, WI38, BJ-ELR, A375, Jurkat, MCF7, T47D, HCT116, PANC-1, SK-MEL28 from ATCC. Becker from JCRB Cell Bank. 005 and RIGH cells were derived at the Salk Institute. GSCs were isolated from specimens of glioblastoma patients who had undergone surgery at the University of Texas MD Anderson Cancer Center. HCT116 p53^{-/-} were a kind gift of Bruno Amati's group.

b. Describe the method of cell line authentication used.

BJ, WI38, BJ-ELR, A375, Jurkat, MCF7, T47D, HCT116, DLD-1, PANC-1, SK-MEL28, Becker were obtained from premier and well recognized cell banks such as ATCC, and the JCRB Cell Bank. No further authentication has been performed. 005 cells were derived at the Salk Institute as tumor cells obtained from mouse glioblastoma multiforme-like tumors. RIG-H1, a mouse GBM cell line, was established at the Salk Institute from a brain tumor that developed in a GFAP-Cre mouse injected with Tomo-Ras-shp53 lentiviral vectors. Both cell lines were tested to confirm that they behave as cancer stem cells as described in PMID: 19122659. GSCs were isolated from specimens of glioblastoma patients who had undergone surgery at the University of Texas MD Anderson Cancer Center. The diagnosis of glioblastoma was established on histological examination according to the WHO classification. Tumor specimens were dissociated and were cultured as neurospheres, and tested for cancer stem cells properties as described in PMID: 15549107 PMID: 14522905.

c. Report whether the cell lines were tested for mycoplasma contamination.

Tested for mycoplasma

d. If any of the cell lines used are listed in the database of commonly misidentified cell lines maintained by [ICLAC](#), provide a scientific rationale for their use.

No cell lines in the list

► Animals and human research participants

Policy information about [studies involving animals](#); when reporting animal research, follow the [ARRIVE guidelines](#)

11. Description of research animals

Provide details on animals and/or animal-derived materials used in the study.

Mice were purchased from The Jackson Laboratories. C57BL/6, NOD.Cg-Prkdcscid1l2rgtm1Wjl 625 /SzJ and Tyr-NrasQ61K males and females between 8-14 weeks old.

Policy information about [studies involving human research participants](#)

12. Description of human research participants

Describe the covariate-relevant population characteristics of the human research participants.

Covariate-relevant population characteristics is not applicable.